

The Maximum Lifetime of the Quark–Gluon Plasma[†]

Dirk H. Rischke[‡] and Miklos Gyulassy

Physics Department, Pupin Physics Laboratories, Columbia University
538 W 120th Street, New York, NY 10027, U.S.A.

September 1995

Abstract

The width ΔT of the deconfinement transition region is shown to influence strongly the flow structure in the (Landau–) hydrodynamical expansion of a quark–gluon plasma. For a sharp first order transition ($\Delta T = 0$) the mixed phase is rather long-lived, with a lifetime that has a maximum when the initial energy density is at the phase boundary between mixed and pure quark–gluon matter. For increasing ΔT , however, the lifetime decreases rapidly. Hadronic matter, however, remains long-lived as a consequence of the rapid change in the degrees of freedom in the transition region and the corresponding “softening” of the equation of state.

[†] This work was supported by the Director, Office of Energy Research, Division of Nuclear Physics of the Office of High Energy and Nuclear Physics of the U.S. Department of Energy under Contract No. DE-FG-02-93ER-40764.

[‡]Partially supported by the Alexander von Humboldt–Stiftung under the Feodor–Lynen program.

1 Introduction

The hydrodynamical approach has been applied extensively to describe the dynamics of relativistic heavy-ion collisions [1, 2, 3], because it provides the only direct link between the equation of state of hot and dense nuclear matter and observable collective flow phenomena. Hydrodynamics is defined by local energy-momentum and (net) charge conservation,

$$\partial_\mu T^{\mu\nu} = 0, \quad \partial_\mu \mathbf{N}^\mu = 0. \quad (1)$$

$T^{\mu\nu}$ is the energy-momentum tensor, N_i^μ the (net) four-current of the i th conserved charge, $\mathbf{N}^\mu = (N_1^\mu, N_2^\mu, \dots, N_m^\mu)$ for m conserved charges. Under the assumption of local equilibrium (the so-called “ideal fluid” approximation) the energy-momentum tensor and the m (net) charge currents assume the particularly simple form [4]

$$T^{\mu\nu} = (\epsilon + p) u^\mu u^\nu - p g^{\mu\nu}, \quad N_i^\mu = n_i u^\mu, \quad i = 1, \dots, m, \quad (2)$$

where ϵ , p , n_i are energy density, pressure, and (net) density of the i th conserved charge in the local rest frame of the fluid, $u^\mu = \gamma(1, \mathbf{v})$ is the four-velocity of the fluid (\mathbf{v} is the three-velocity, $\gamma \equiv (1 - \mathbf{v}^2)^{-1/2}$, $u_\mu u^\mu = 1$), and $g^{\mu\nu} = \text{diag}(+, -, -, -)$ is the metric tensor¹. The system of $m + 4$ equations (1) is closed via eliminating one of the $m + 5$ unknowns in eqs. (2) by choosing an equation of state e.g. in the form $p = p(\epsilon, n_1, \dots, n_m)$. In the ideal fluid approximation, the (equilibrium) equation of state is the *only* input to the hydrodynamical equations of motion (1) that relates to properties of the matter under consideration and is thus able to influence the dynamical evolution of the system. The final results are uniquely determined once a particular initial condition and a decoupling (“freeze-out”) hypersurface are specified.

In ultrarelativistic heavy-ion collisions ($\sqrt{s} \sim 200$ AGeV), the central region (in the center-of-momentum frame) is essentially free of (net) charges, due to the insufficient amount of baryon stopping [5], and the charge conservation equations in (1) do not have to be solved explicitly to describe the fluid evolution in this particular region of space-time. Moreover, the equation of state depends only on a single independent thermodynamical variable, for instance the temperature T . From the pressure as a function of T , $p(T)$, one derives the entropy density $s \equiv dp/dT$, and the energy density $\epsilon \equiv Ts - p$.

For this particular case, lattice QCD calculations [6] provide fundamental information on the equation of state of strongly interacting matter. These calculations [7] show a rapid increase of the entropy density as a function of temperature, $s(T)$, in a narrow temperature interval $\Delta T \sim 10$ MeV around a temperature $T_c \simeq 150$ MeV, indicating the presence of a transition from hadronic degrees of freedom at low temperatures to quark and gluon degrees of freedom at high temperatures. For a first order phase transition, the increase in s is actually a discontinuity, and ΔT is zero, while for a second or higher order transition the change of the entropy density is continuous, and ΔT is finite. Thusfar, however, lattice calculations have not converged on the order of the QCD phase transition [8, 9, 10], and we only know that $\Delta T \leq 0.1 T_c$.

¹Our units are $\hbar = c = k_B = 1$.

In this paper we discuss the sensitivity of the structure of hydrodynamic flow to this uncertainty in the equation of state. To this end we treat the width ΔT of the transition region as a free parameter and assume the following functional form for the entropy density [11],

$$s(T) = c_H T^3 \frac{1 - \tanh[(T - T_c)/\Delta T]}{2} + c_Q T^3 \frac{1 + \tanh[(T - T_c)/\Delta T]}{2}. \quad (3)$$

Other functional forms are, of course, also possible and eq. (3) is chosen only for the sake of simplicity. For $T \ll T_c$, the entropy density becomes that of a hadron gas, $s(T) \simeq c_H T^3$, while for $T \gg T_c$, it assumes the value for a quark–gluon plasma, $s(T) \simeq c_Q T^3$. We denote the ratio of degrees of freedom in the quark–gluon and hadron phases by $r \equiv c_Q/c_H$. If the hadron phase is taken to be an ideal, massless pion gas, and the quark–gluon plasma to consist of (non-interacting, massless) u and d quarks and gluons, then $r = 37/3$. In the limit $\Delta T \rightarrow 0$ the equation of state (3) features a first order phase transition between the two phases at the phase transition temperature T_c and reduces to the MIT bag model equation of state [12]. In this paper we vary ΔT between 0 and $0.1 T_c$, consistent with the uncertainties in present lattice QCD data.

The first study of the sensitivity of hydrodynamic flow on ΔT was done in [11]. It was found that for $\Delta T < \Delta T^*$, where $\Delta T^* \simeq 0.07 T_c$, matter is thermodynamically anomalous in the phase transition region and, consequently, that rarefaction shock waves occur in the one–dimensional expansion [13, 14]. On the other hand, for $\Delta T \geq \Delta T^*$, matter is thermodynamically normal everywhere and simple rarefaction waves form the hydrodynamically stable solution. The main result of Ref. [11], however, was that, for the particular initial conditions chosen in that work, those structural differences had little effect on the final flow pattern. This led the authors of [11] to the conclusion that observables, such as the distribution of outgoing particles, would hardly be affected by the uncertainty in ΔT .

Renewed interest in the sensitivity of hydrodynamic flow on the equation of state has arisen as a consequence of the work of Refs. [14, 15, 16]. It was demonstrated that a phase transition leads to a so-called [15] “softest point” in the equation of state, defined by a minimum in the ratio p/ϵ . For the equation of state (3) with $\Delta T = 0$, this point occurs at the phase boundary between mixed and pure quark–gluon matter (see also Section 2). It was argued [15] that at this point the comparatively small pressure prevents a fast expansion and cooling of the system. This leads to a maximum in the lifetime of mixed phase matter as a function of the initial energy density. On this basis it was suggested [15] that the resulting enhanced emission of electromagnetic probes from this long-lived mixed phase could serve as a signature for the creation of the quark–gluon plasma in ultrarelativistic heavy–ion collisions.

In Ref. [16], the suppressed tendency for expansion at the softest point was shown to cause a minimum in the excitation function of the directed transverse collective flow in semi-peripheral collisions. It was proposed that this minimum would also be a unique signature for the phase transition. Another important observable sensitive to the lifetime of the plasma is pion interferometry [17]. In the standard “slowly burning log” scenario inspired by the small deflagration velocities associated with sharp transitions [18] one expects a dramatic difference between “out”– and “side”–correlations, which could serve as a signal of the phase

transition.

In the present work, we investigate the hydrodynamic flow pattern for one-dimensional expansion in greater detail than in [11]. In particular, we focus on the question of the lifetime of different parts of the system as a function of the initial energy density ϵ_0 and the width ΔT of the transition region. While one-dimensional hydrodynamics is not realistic for a detailed comparison with heavy-ion data, its simplicity allows us to study the influence of the equation of state on the hydrodynamic flow without additional effects originating from more complicated geometries.

We confirm the observation made in [11] that, for initial energy densities well above or below the softest point of the equation of state, the temperature profiles in the thermodynamically normal case ($\Delta T \geq \Delta T^*$) look indeed similar to those in the thermodynamically anomalous case ($\Delta T < \Delta T^*$). However, we demonstrate that the temperature profiles are quite sensitive to a variation of ΔT for ϵ_0 *near* the softest point of the equation of state. In particular, the lifetime of matter with temperatures near T_c decreases rapidly for increasing ΔT . On the other hand, the lifetime of matter with temperatures well below T_c remains large and may even grow for increasing ΔT . This is due to the “softening” of the equation of state by the change of degrees of freedom across the transition region. Thus, the detectability of the quark-gluon plasma via enhanced emission of electromagnetic probes may depend sensitively on ΔT , while other observables such as flow and correlation functions are expected to remain fairly insensitive to that uncertainty.

This paper is organized as follows. In Section 2 we review properties of the equation of state (3) in greater detail and establish the connection to thermodynamically normal or anomalous behaviour. Section 3 presents the expansion solutions as functions of ϵ_0 and ΔT . In Section 4 we discuss the lifetimes of parts of the system having different temperatures. Section 5 concludes this work with a summary of our results.

2 Equation of state and thermodynamical behaviour

In this section we discuss the equation of state (3) and its thermodynamical properties. The entropy density at the phase transition temperature is $s_c \equiv s(T_c) = c_H(r+1)T_c^3/2$. With the definition $\rho \equiv (r+1)/(r-1)$ and $\Theta(T) \equiv (T - T_c)/\Delta T$, one can write [11]

$$\frac{s}{s_c}(T) = \left[\frac{T}{T_c} \right]^3 \left(1 + \rho^{-1} \tanh \Theta(T) \right) , \quad (4)$$

and subsequently obtains pressure and energy density from

$$p(T) = \int_0^T dT' s(T') , \quad \epsilon(T) = T s(T) - p(T) . \quad (5)$$

The square of the velocity of sound is

$$c_s^2 \equiv \frac{dp}{d\epsilon} = \frac{s}{T} \frac{dT}{ds} = \left(3 + \frac{T}{\Delta T} \frac{1}{\rho + \tanh \Theta(T)} \frac{1}{\cosh^2 \Theta(T)} \right)^{-1} . \quad (6)$$

It is obvious that for $T \ll T_c$ or $T \gg T_c$ (or, equivalently, $|\Theta(T)| \gg 1$) the velocity of sound approaches the value for an ultrarelativistic ideal gas, $c_s = 1/\sqrt{3}$. In the transition region, c_s decreases and has a minimum. In the limit $\Delta T \rightarrow 0$, c_s approaches zero at $T = T_c$ and assumes the ideal gas value elsewhere. In Fig. 1 we show the energy density, the pressure, the entropy density, and the square of the velocity of sound as functions of temperature. Note that above T_c , the energy density approaches the Stefan–Boltzmann value for a quark–gluon gas from above, while the pressure approaches it rather slowly from below. Both phenomena are observed in lattice data [7], and are a consequence of general thermodynamical relationships [19].

A way to classify the structure of one–dimensional hydrodynamical solutions [13, 14] is through the sign of

$$\Sigma \equiv \frac{d^2 p}{d\epsilon^2} + \frac{2c_s^2(1 - c_s^2)}{\epsilon + p}. \quad (7)$$

(An equivalent classifying quantity is the curvature of the Poisson adiabat [11].) For the equation of state (3) we obtain

$$\Sigma T s = 3c_s^2(1 - 3c_s^2) \left[1 + \frac{4c_s^4}{1 - 3c_s^2} + \frac{2}{3}c_s^2 \frac{T}{\Delta T} \tanh \Theta(T) \right]. \quad (8)$$

Matter is called thermodynamically normal if Σ is positive and thermodynamically anomalous if it is negative. It was shown in [11, 13, 14] that in the first case the hydrodynamically stable solution for the one–dimensional expansion of semi-infinite matter is a simple rarefaction wave, while in the latter case it is a rarefaction shock wave. Depending on the value of ΔT , the equation of state (3) features thermodynamically normal as well as thermodynamically anomalous regions, as discussed below. The hydrodynamical solution for the one–dimensional expansion of semi-infinite matter may thus consist of a sequence of simple waves and shocks. For the one–dimensional expansion of finite matter, the expansion solution is that for semi-infinite matter as long as the rarefaction waves have not reached the center of symmetry of the system (usually taken to be the center of the coordinate system, $x = 0$). Afterwards, the solution no longer consists only of simple waves and shocks but is more complicated (see also next section). An analytic solution is so far only known for thermodynamically normal matter with a constant velocity of sound [20].

To see where matter described by (3) becomes thermodynamically anomalous, it is advantageous to plot thermodynamic quantities as a function of the energy density, since in the case $\Delta T = 0$, the mapping $T \rightarrow \epsilon(T)$ is not one-to-one. Moreover, the beam energy fixes the initial energy density, while the initial temperature is determined only indirectly through the equation of state. In Fig. 2 we show the entropy density, the ratio p/ϵ , the velocity of sound (squared), and $\Sigma T s$ as functions of ϵ . Fig. 2 (b) serves to elucidate the notion of a “softest point” of an equation of state. For $\Delta T = 0$, $p/\epsilon = 1/3 \equiv c_s^2 = \text{const.}$ in the hadronic phase. At the phase boundary between hadronic and mixed phase, $\epsilon_H \equiv 3T_c s_c/2(r+1) = 0.1125 T_c s_c$ (for our choice of $r = 37/3$), the ratio p/ϵ starts to decrease, since $p \equiv p_c = T_c s_c/2(r+1) = \text{const.}$ in the mixed phase while ϵ increases. At the phase boundary between mixed and quark–gluon matter, $\epsilon_Q \equiv (4r-1)T_c s_c/2(r+1) = 1.8125 T_c s_c$ (for $r = 37/3$), p/ϵ assumes a minimum which is the so-called “softest point” [15]. In the

quark–gluon phase, p/ϵ increases again and reaches the asymptotic value $1/3 \equiv c_s^2$ for $\epsilon \rightarrow \infty$. For increasing ΔT , the softest point is shifted towards smaller values of ϵ . In addition, the equation of state becomes “less soft” at that point, i.e., the minimum value of p/ϵ increases. On the other hand, there is a “softening” at energy densities around ϵ_H .

Figs. 2 (c,d) show that, for $\Delta T = 0$, the velocity of sound and Σ vanish in the mixed phase, $\epsilon_H \leq \epsilon \leq \epsilon_Q$. Although matter with a vanishing Σ is not thermodynamically anomalous in a rigorous sense, this nevertheless suffices to produce a rarefaction shock wave in the expansion [14, 21]. For ΔT being finite, but smaller than a critical value² $\Delta T^* \simeq 0.07676 T_c$, there are always regions where Σ becomes negative, i.e., where the equation of state is thermodynamically anomalous, and consequently, where rarefaction shock waves appear in the expansion. For ΔT larger than ΔT^* , matter is thermodynamically normal everywhere and simple rarefaction waves form the hydrodynamically stable solution. Nevertheless, since the velocity of sound varies appreciably in the transition region, Fig. 2 (c), there will be modifications to a simple wave profile calculated with a constant velocity of sound.

Note especially in Fig. 2 (d) that the region where matter becomes thermodynamically anomalous shrinks drastically even for tiny ΔT . To understand this we first expand the velocity of sound squared (6) for small $\Delta T/T_c \ll 1$ in the vicinity of $T = T_c$,

$$c_s^2 \simeq \frac{\Delta T/T_c}{T/T_c} \frac{\rho + \tanh \Theta(T)}{1 - \tanh^2 \Theta(T)}. \quad (9)$$

Note that $\Theta(T) \equiv (T - T_c)/\Delta T$ is *not* necessarily small in this limit, i.e., one *must not* expand the hyperbolic tangents in this expression. In accord with Figs. 1 (d) and 2 (c), c_s^2 is of the order $\Delta T/T_c \ll 1$ near T_c . Next, we determine the roots of eq. (8) to lowest order in the small quantities $\Delta T/T_c$ and $T/T_c - 1$. This yields a quadratic equation for $\tanh \Theta(T)$ with only one physical solution $\tanh \Theta(T_\Sigma) = \rho - (\rho^2 + 3)^{1/2} \simeq -0.9173$, corresponding to the upper boundary of the region where matter is thermodynamically anomalous. The lower boundary cannot be obtained in our approximation, because c_s^2 is already large in the respective region of energy densities, cf. Figs. 2 (c,d). Since $\tanh \Theta(T_\Sigma)$ is of order unity, an expansion of the hyperbolic tangent in (9) is indeed not possible. Note that $T_\Sigma/T_c - 1 \equiv (\Delta T/T_c) \text{Arctanh}[\rho - (\rho^2 + 3)^{1/2}] \simeq -1.572 \Delta T/T_c$. Thus, matter with temperature $T = T_c$ is always thermodynamically normal for finite ΔT . Finally, we calculate the energy density corresponding to the upper boundary to lowest order,

$$\begin{aligned} \epsilon_\Sigma &\simeq T_c s_c (1 + \rho^{-1} \tanh \Theta(T_\Sigma)) - p_c = \epsilon_c + T_c s_c \left(1 - \sqrt{1 + 3\rho^{-2}}\right) \\ &= 0.18275 T_c s_c \ll \epsilon_Q = 1.8125 T_c s_c, \end{aligned} \quad (10)$$

where $\epsilon_c \equiv T_c s_c - p_c = (2r + 1) T_c s_c / 2(r + 1) = 0.9625 T_c s_c$. (This is the point where all curves in Fig. 1 (a) intersect.) This result is remarkable in several aspects. First, the fact that $\tanh \Theta(T_\Sigma)$ is not small leads to a large shift of ϵ_Σ away from the point ϵ_c *already to zeroth order in $\Delta T/T_c$* . We checked numerically that first order corrections in $\Delta T/T_c$ do not change the value for ϵ_Σ appreciably before our approximations break down anyway. Second,

²This value was found numerically using eq. (8).

this shift is *negative*, i.e., away from ϵ_Q which is the upper boundary in the case $\Delta T = 0$. Thus, the size of the region where matter is thermodynamically anomalous does not change continuously in the limit $\Delta T \rightarrow 0$, but increases abruptly when going from arbitrarily small ΔT to $\Delta T = 0$. In this sense, the case $\Delta T \equiv 0$ is very special in that it features an exceptionally large region where matter is thermodynamically anomalous.

3 One-dimensional expansion solutions

In this section the one-dimensional hydrodynamic expansion of a finite slab of matter with (homogeneously distributed) initial energy density ϵ_0 is investigated with emphasis on the dependence of the flow structure on ϵ_0 and ΔT . To solve the hydrodynamic equations (1) in (1+1)-dimensions we employ the relativistic Harten-Lax-van Leer-Einfeldt (HLL E) algorithm presented in [14, 22] with a grid spacing of $\Delta x = 0.025 R$ ($2 R$ being the initial size of the slab) and a time step width of $\Delta t = 0.99 \Delta x$. This algorithm was shown [14] to accurately reproduce hydrodynamic flow profiles for analytically solvable test problems where the equation of state has thermodynamically normal as well as anomalous regions. In particular, for the choice $\Delta x = 0.025 R$, the algorithm accurately reproduced the expansion solution for a finite system of size $2 R$ consisting of thermodynamically normal matter with a constant velocity of sound. (This solution was first provided by Landau in purely analytical form [20], but can also be easily constructed semi-analytically via the method of characteristics [23].)

In the following Figs. 3 – 7 we demonstrate how the flow structure changes systematically in the range $\epsilon_H \leq \epsilon_0 \leq 10 \epsilon_Q$ and for various ΔT . Each figure corresponds to a fixed ϵ_0 , and shows the time evolution of temperature, center-of-momentum frame (CM) energy density, and the space-time structure of isotherms³ in three columns corresponding to $\Delta T = 0, 0.01 T_c$, and $0.1 T_c$.

3.1 $\epsilon_0 = \epsilon_H$

In Fig. 3 we show the expansion solution for an initial energy density $\epsilon_0 \equiv \epsilon_H = 3 T_c s_c / 2(r + 1) = 0.1125 T_c s_c$. For $\Delta T = 0$, Figs. 3 (a,d,g), this energy density corresponds to the boundary between hadronic and mixed phase matter. Thus, thermodynamically anomalous regions of the equation of state are not reached during the expansion, and the expansion proceeds at first as a simple rarefaction wave. After this simple wave overlaps with its symmetric counterpart coming from the ($-x$)-direction, the hydrodynamical solution is identical to that given by Landau [20].

For $\Delta T = 0.01 T_c$, Figs. 3 (b,e,h), the expansion seems to proceed rather similar to the previous case. Fig. 2 (d) shows, however, that around $\epsilon_0 = \epsilon_H$ the equation of state has a region where matter is thermodynamically anomalous. Thus, a rarefaction shock wave is bound to form in the expansion. Since the anomalous region is confined to a very narrow

³For $\Delta T = 0$ all states of mixed phase matter have the same temperature T_c , cf. Fig. 1 (a). In this case, we define the ($T = T_c$)-isotherm as the set of space-time points where T has just infinitesimally dropped below T_c [14].

range about ϵ_H , cf. Fig. 2 (d), the shock is weak and difficult to resolve numerically. The best evidence for its existence can be found in Fig. 3 (e), in that the slope of the rarefaction wave travelling into the slab is steeper than in the corresponding Figs. 3 (d,f) where no shock occurs.

For $\Delta T = 0.1 T_c$, Figs. 3 (c,f,i), matter is thermodynamically normal everywhere, cf. Fig. 2 (d). Consequently, the expansion initially proceeds as a simple rarefaction wave, as for $\Delta T = 0$. For such a wave, the matter velocity with respect to the wave profile equals the velocity of sound [4, 14]. Thus, the head of the simple wave travels with the velocity of sound c_s into matter which is initially at rest. In the respective range of energy densities, c_s is considerably smaller for $\Delta T = 0.1 T_c$ than for $\Delta T = 0$, cf. Fig. 2 (c). Therefore, as can be clearly seen in Figs. 3 (c,f), it takes much longer for the simple rarefaction wave to reach the center $x = 0$ than in Figs. 3 (a,d). The delayed rarefaction can be also seen comparing Figs. 3 (g) and (i): it takes about $4R$ for the system at $x = 0$ to cool below $T = 0.7 T_c$ and about $6R$ to cool below $T = 0.5 T_c$, while the corresponding values for $\Delta T = 0$ are $3R$ and $5R$.

The reason why there is no $(T = T_c)$ -isotherm in Fig. 3 (h) and no $(T = T_c)$ - and $(T = 0.9 T_c)$ -isotherm in Fig. 3 (i) can be inferred from Fig. 1 (a): as long as the energy density is below $\epsilon_c \equiv (2r + 1) T_c s_c / 2(r + 1) = 0.9625 T_c s_c$, the temperature corresponding to that energy density is smaller for larger ΔT . Thus, for $\Delta T = 0.01 T_c$, already the initial temperature is below T_c , and for $\Delta T = 0.1 T_c$ even below $0.9 T_c$, cf. Figs. 3 (b,c). Therefore, there simply are no corresponding isotherms in the space-time diagram.

Note that the temperature and CM energy density profiles show a minimum at $x = 0$ for late times t . As was explained in [14], this is essentially a relativistic effect. At finite x , matter is moving, while due to symmetry it is at rest at $x = 0$. Moving matter, however, experiences relativistic time dilation and is thus less diluted and still hotter at a given time in the CM frame than matter at rest. Of course, the degree of dilation a fluid element experiences is determined by its velocity. This velocity is, in turn, determined by the “stiffness” of the equation of state, i.e., the ratio of pressure to energy density, since that ratio influences the acceleration of fluid elements. Thus, for the typical energy densities occurring in Fig. 3, matter velocities are smaller for larger values of ΔT , since the equation of state is softer, cf. Fig. 2 (b). This explains why the minimum at $x = 0$ (or the time dilation effect, respectively) is less pronounced (and occurs at later times) in Figs. 3 (c,f) than for instance in Figs. 3 (a,d).

3.2 $\epsilon_H < \epsilon_0 < \epsilon_Q$

Fig. 4 shows the time evolution of temperature and CM energy density, and the isotherms in the space-time diagram for an initial energy density $\epsilon_0 = 30 T_c s_c / 2(r + 1) = 1.125 T_c s_c$, i.e., $\epsilon_H < \epsilon_0 < \epsilon_Q = (4r - 1) T_c s_c / 2(r + 1) = 1.8125 T_c s_c$. For $\Delta T = 0$, Figs. 4 (a,d,g), the initial state is thermodynamically anomalous mixed phase matter. Therefore, rarefaction proceeds via a shock wave, in front of which mixed phase matter is at rest. Hadronic matter emerges from the shock in an accelerated state and is subsequently diluted by a simple rarefaction wave [14]. Note that the shock velocity is quite small, leading to a long lifetime of $\sim 26R$ for mixed phase matter at $x = 0$. We can understand the value for the lifetime

from the expression for the rarefaction shock velocity, eq. (70) of Ref. [14], which reduces, for $\epsilon_H \ll \epsilon_0 \leq \epsilon_Q$, to

$$v_{sh} \simeq -\frac{2}{3\sqrt{3}\epsilon_0/\epsilon_H} \simeq -(2.6\epsilon_0/\epsilon_H)^{-1}. \quad (11)$$

Therefore, we expect for $\epsilon_0/\epsilon_H = 2(r+1)\epsilon_0/3T_c s_c = 10$ a lifetime $t_{life} \equiv R/|v_{sh}| \simeq 26R$, in accord with Fig. 4 (g).

Again, the expansion for $\Delta T = 0.01 T_c$ looks similar, especially the temperature profiles, cf. Figs. 4 (a) and (b). The difference is that now the initial energy density is well above the region where matter is thermodynamically anomalous, cf. Fig. 2 (d). Therefore, the expansion has at first to proceed as a simple rarefaction wave, until the energy density has dropped sufficiently to reach that region. Then, a rarefaction shock wave provides further dilution. This can be most clearly seen in the CM energy density profiles, Fig. 4 (e). The reason why the temperature profiles, Fig. 4 (b), do not clearly exhibit this behaviour is that T is proportional to a fractional power of ϵ , so that the range of high energy densities is not well resolved when plotted as a function of temperature. A clear indication for this behaviour, however, can be found comparing the space–time diagram Fig. 4 (g), where the $(T = 0.9 T_c)$ – and $(T = T_c)$ –isotherms coincide, since both temperatures occur at the position of the shock, with Fig. 4 (h), where they are well separated due to the simple rarefaction wave preceding the shock. Note that this has a drastic influence on the lifetime of matter with $T = T_c$. Such matter is thermodynamically normal for finite ΔT , as discussed in the context of Fig. 2 (d), and consequently rapidly diluted by the simple rarefaction wave. The lifetime drops by more than a factor of 2 as compared to Fig. 4 (g). On the other hand, the lifetime of matter with $T = 0.9 T_c$ remains comparable to that in the case $\Delta T = 0$, since this temperature occurs on the rarefaction shock front, cf. Fig. 4 (b), as was also the case in Fig. 4 (a). We will discuss this phenomenon in more detail in the next section.

For $\Delta T = 0.1 T_c$, Figs. 4 (c,f,i), matter is thermodynamically normal everywhere and the hydrodynamically stable rarefaction solution is a simple wave (until it reaches the center $x = 0$ and overlaps with its counterpart from the $(-x)$ –region). Nevertheless, due to the variation of the velocity of sound in the phase transition region, cf. Fig. 2 (c), the shape of the simple wave exhibits a “bump” faintly resembling a smeared version of the rarefaction shock occurring in the previous two cases. This bump, however, is moving rapidly in positive x –direction, in contrast to the rarefaction shock in Fig. 4 (b), which is approximately stationary, or that in Fig. 4 (a), which is even slowly moving in $(-x)$ –direction. This has the effect that the hot parts of the system ($T \geq 0.9 T_c$) cool faster than in the two previous cases. This can be understood with the help of Fig. 2 (b) which shows that for the respective energy densities the equation of state is “stiffer” for increasing ΔT , thus increasing the system’s tendency to expand and cool.

On the other hand, the cooler parts ($T \leq 0.7 T_c$) keep their temperature longer for $\Delta T = 0.1 T_c$, cf. also Figs. 4 (g,h,i). The reason is that the equation of state for small energy densities (low temperatures) is softer than in the other two cases, cf. Fig. 2 (b). Thus, the acceleration and consequently the matter velocities are smaller, and therefore the rarefaction and cooling take longer. We finally mention that, since now $\epsilon_0 > \epsilon_c$, the initial temperature increases with ΔT , cf. Fig. 1 (a), in contrast to the previous case, Fig. 3.

3.3 The softest point $\epsilon_0 \sim \epsilon_Q$

Fig. 5 shows the expansion solutions for $\epsilon_0 = 50 T_c s_c / 2(r + 1) = 1.875 T_c s_c$. For $\Delta T = 0$, Figs. 5 (a,d,g), this energy density is just above the softest point of the equation of state, i.e., the phase boundary between mixed and pure quark–gluon matter, $\epsilon_Q \equiv (4r - 1)T_c s_c / 2(r + 1) = 1.8125 T_c s_c$. Consequently, a simple rarefaction wave precedes the rarefaction shock wave travelling into hot quark–gluon matter [14]. (The simple rarefaction wave is not visible in Fig. 5 (a) due to the large time step chosen.) This has the consequence that matter is pre-accelerated before it enters the shock wave. In conjunction with the equation of state becoming increasingly stiffer for smaller energy densities in the mixed phase, cf. Fig. 2 (b), this has the further consequence that the CM energy density develops a minimum at $x = 0$ for given t , cf. Fig. 5 (d), just as in Fig. 3. We note that, in agreement with the results of [14], the rarefaction shock is almost stationary for an ϵ_0 this close to the softest point of the equation of state. This leads to a (local) maximum for the lifetime of matter with $T = T_c$ at $x = 0$. The particular value in Fig. 5 (g) can be again understood with the help of the approximate formula (11) which gives⁴ $t_{life} \simeq R/|v_{sh}| \simeq 43 R$.

The temperature profiles for $\Delta T = 0.01 T_c$, Fig. 5 (b), look again similar to that of Fig. 5 (a), although the shock wave is no longer stationary, but at first advancing in x -direction. The reason is that the shock strength is smaller than in the previous case (due to the much narrower region where matter is thermodynamically anomalous, cf. Fig. 2 (d)), which is especially obvious from comparing Figs. 5 (d) and (e). Therefore, the velocity of the shock, which is originally directed inwards, is too small to compete with the pre-acceleration of matter in the simple rarefaction wave preceding the shock, resulting in a net outward motion of the shock. This mechanism is also responsible for the positive shock velocity observed for higher ϵ_0 in the cases $\Delta T = 0$ and $0.01 T_c$, see Figs. 6, 7 below. For later times, however, just before the high energy density matter in the center is completely consumed, the shock reverses its direction, due to the fact that the energy density (or pressure) in the interior has now become too small to keep it driving outwards. (This effect is also visible in Fig. 5 (a).)

The energy density profiles, Fig. 5 (e), do not show the minimum at $x = 0$ typical for relativistic time dilation of moving matter. The reason is that in this case the equation of state is soft for the respective energy densities, cf. Fig. 2 (b). As explained above, this leads to small (i.e. non-relativistic) matter velocities and the absence of an appreciable amount of time dilation.

The expansion for $\Delta T = 0.1 T_c$, Fig. 5 (c,f) resembles the corresponding one in Figs. 4 (c,f). In particular, the “bump” structure caused by the variation of the velocity of sound is again clearly visible. As in Fig. 4, however, the expansion differs appreciably from the one for $\Delta T = 0$ and $0.01 T_c$ in Figs. 5 (a,b,d,e).

The relative time scales of cooling are similar to the previous case $\epsilon_0 = 1.125 T_c s_c$, cf. Figs. 4 (g,h,i) with Figs. 5 (g,h,i). Note again the sharp decrease in the lifetime of matter with $T = T_c$ for $\Delta T = 0.01 T_c$ as compared to the case $\Delta T = 0$, while matter with $T = 0.9 T_c$ remains long-lived. For $\Delta T = 0.1 T_c$, also the lifetime of matter with temperature $T = 0.9 T_c$

⁴We may safely neglect the small pre-acceleration of matter due to the simple rarefaction wave preceding the shock in the quark–gluon phase.

is reduced, while matter that is even cooler still lives longer.

3.4 $\epsilon_0 \sim 2 \epsilon_Q$

Fig. 6 shows the expansion for an initial energy density $\epsilon_0 = 100 T_c s_c / 2(r + 1) = 3.75 T_c s_c \sim 2 \epsilon_Q$. This case is of interest since for initial energy densities of this order of magnitude a rather peculiar phenomenon occurs in the expansion for an equation of state with $\Delta T = 0$. One observes in Figs. 6 (a,d) that the rarefaction shock wave is now driven outwards by the pre-acceleration from the simple rarefaction wave, as was already discussed above. Matter behind the shock experiences cooling typical for the Landau expansion with a sufficiently stiff equation of state, i.e., slower matter near the center $x = 0$ cools more rapidly than faster matter at larger $x = 0$. This, however, has the consequence that as soon as the (comoving) energy density drops below ϵ_H , or equivalently, the temperature drops below T_c , a second rarefaction shock wave develops that connects hadronic matter in the center with mixed phase matter behind the first shock.

The occurrence of the second shock could have been expected, since matter changes from thermodynamically anomalous in the mixed phase to thermodynamically normal in the hadron phase. To our knowledge there is now, however, no general mathematical theorem rigorously proving the existence of this second shock, as was the case in the expansion of semi-infinite matter studied in [14]. The shock has an interesting further consequence: just as the first shock expels hadronic matter outwards, the second accelerates matter *inwards*. Therefore, there is an accumulation of matter in the center which is consequently *reheated* instead of cooled. This reheating of the center can be clearly seen in Fig. 6 (g), where the triangle-shaped isotherm at small x and $t \sim 70 R$ is a *re-occurrence* of the ($T = 0.9 T_c$)–isotherm caused by reheating. In addition, also the ($T = 0.7 T_c$)–isotherm shows that the central region remains hot over a much longer period of time than for the expansion of matter without a phase transition.

The reheating is considerably smaller for $\Delta T = 0.01 T_c$, cf. Figs. 6 (b,e,h), and basically only discernible from the shape of the ($T = 0.7 T_c$)–isotherm. The reason is, of course, that the region in the equation of state, where matter is thermodynamically anomalous, is much narrower, cf. Fig. 2 (d), so that the strength of the second rarefaction shock is smaller and consequently the acceleration of matter towards the center much weaker. For $\Delta T = 0.1 T_c$ there is no such an effect at all, and the fluid evolution is rather different from the cases $\Delta T = 0$ and $0.01 T_c$.

3.5 $\epsilon_0 \gg \epsilon_Q$

Finally, we show in Fig. 7 the expansion for $\epsilon_0 = 500 T_c s_c / 2(r + 1) = 18.75 T_c s_c \gg \epsilon_Q$. This case is similar to the one studied in Fig. 13 in Ref. [11], although we followed the fluid evolution over a much longer time. Here, the acceleration from the simple wave travelling into the quark–gluon phase is rather large, leading to a shock wave in Figs. 7 (a,b,d,e) that is rapidly moving outwards. Note that now also the temperature profiles for $\Delta T = 0.1 T_c$, Fig. 7 (c), resemble those in the case $\Delta T = 0$, Fig. 7 (a) (with the exception of the immediate vicinity of the rarefaction shock). The main reason is that the fluid motion is now

dominated by the conversion of the large initial energy density into collective motion, so that the influence of the phase transition region on the structure of the hydrodynamic solution becomes less important. Moreover, as in the cases considered previously, the variation of the velocity of sound in the phase transition region causes a “bump” structure that resembles a smeared shock.

The similarity of the temperature profiles in Figs. 7 (a) and (c) led the authors of [11] to the conclusion that final state observables will not be much influenced by the precise value of ΔT . They reached the same conclusion studying the expansion with an initial entropy density $s_0 = 0.3 s_c$ (Fig. 11 in [11]) which corresponds, for $\Delta T = 0$, to an initial energy density $\epsilon_0 = 0.2625 T_c s_c$. For this case, the expansion is similar to the one studied here in Fig. 3. That figure shows that the influence of ΔT on the expansion is negligible also for such small initial energy densities, confirming the conclusions of [11]. As we have seen, however, the profiles are *rather* sensitive to the choice of ΔT for initial energy densities *near the softest point of the equation of state*. In particular, the reheating phenomenon of Figs. 6 (a,d,g) does not occur at all for $\Delta T = 0.1 T_c$, cf. Figs. 6 (c,f,i). We discuss the effect on the lifetime of matter with different temperatures in the next section.

4 Lifetime of parts of the system having different temperatures

In this section we discuss the lifetimes of parts of the system having different temperatures. The “lifetime” is defined as the time it takes the system to cool below a certain temperature T^* at $x = 0$. More precisely, the “lifetime” is the intercept of the isotherm $t(x; T^*)$ in the $(t - x)$ -plane with the t -axis, i.e., $t_{life} \equiv t(0; T^*)$. We choose the point $x = 0$ to measure this time, since the motion of fluid cells at finite x causes a time dilation which leads to a slower cooling when measured in the global CM frame of the system. In case there is more than one intercept, for instance when there is reheating of the center, Fig. 6 (g), we choose the first.

We investigate the lifetime in two different geometries. In subsection 4.1 we study longitudinal expansion for fixed initial “radius” R of the system. In subsection 4.2 we investigate a more realistic geometry where the initial longitudinal size R takes into account the Lorentz contraction of the colliding nuclei. Thus, R varies with beam energy, and hence with the initial energy density ϵ_0 .

4.1 Fixed R

In Fig. 8 we show the lifetime of parts of the system having temperature $T = 0.5 T_c, 0.7 T_c, 0.9 T_c, T_c, 1.1 T_c, \text{ and } 1.3 T_c$ for the three different $\Delta T = 0, 0.01 T_c, 0.1 T_c$, and for an ideal gas equation of state without phase transition and constant velocity of sound $c_s = 1/\sqrt{3}$ as a function of the initial energy density ϵ_0 . We measure the lifetime in units of R . For the ideal gas calculation, Fig. 8 (d), there is of course no phase transition, and the temperature scale set by T_c is arbitrary. The results of Fig. 8 (d) were obtained using $T_0/T_c \equiv (4 \epsilon_0/3 T_c s_c)^{1/4}$.

One observes that for initial energy densities smaller than $\sim \epsilon_c$, the lifetime of matter with temperatures $T \leq 0.9 T_c$ is essentially independent of ΔT . The only exception is that for $\Delta T = 0$ and $0.01 T_c$ the lifetime of matter having $T = 0.7 T_c$ and $T = 0.9 T_c$ is equal, while that is not the case for $\Delta T = 0.1 T_c$. The reason is obvious from Figs. 4, 5: in the first two cases the rarefaction shock wave, once it reaches the center, abruptly cools matter to about $0.5 T_c$, thus terminating the existence of matter having $T = 0.9 T_c$ as well as $T = 0.7 T_c$ simultaneously. This can be clearly seen in the space–time diagrams Figs. 4, 5 (g) and (h). In the case $\Delta T = 0.1 T_c$, rarefaction proceeds via simple waves which are continuous solutions and gradually cool the system, and thus matter with $T = 0.7 T_c$ survives longer than hotter matter with $T = 0.9 T_c$.

The second observation is that the lifetime of “very hot” parts of the system, i.e., matter having temperature $T = 1.1 T_c$ and $1.3 T_c$, is also comparable for all three values of ΔT . These high temperatures occur, of course, only for sufficiently high initial energy densities. The reason for the similarity in the lifetimes is that a variation of ΔT has little effect on the equation of state for high energy densities (or temperatures), cf. Fig. 1. Consequently, also the fluid evolution must be similar for these high temperatures .

For initial energy densities near the softest point of the equation of state and for temperatures around T_c , however, ΔT has an appreciable influence on the lifetime. For instance, one clearly observes in Fig. 8 (a) that the lifetime of matter with $T = 0.9 T_c$ and $T = T_c$ has a maximum near the softest point, cf. Fig. 2 (b). This effect was discussed in detail in Ref. [14] and in the context of Fig. 5 above. It has been explained by the existence of a minimum in the velocity of the rarefaction wave travelling into the system, leading to the “slow burning” of hot matter also observable in Figs. 4, 5 (a,d). An alternative explanation was given in [15], namely that the small p/ϵ –ratio at this point reduces the system’s tendency to expand.

However, Figs. 8 (b,c) show that this maximum in the lifetime is rapidly washed out and eventually vanishes for increasing ΔT , although the p/ϵ –ratio still exhibits a minimum, cf. Fig. 2 (b). This vanishing of the maximum in the lifetime of matter with a particular temperature is essentially explained by a gradual *reduction* of the lifetime when increasing ΔT : first, the lifetime of matter with $T = T_c$ is reduced when increasing ΔT from 0 to $0.01 T_c$, cf. Figs. 8 (a) and (b). Then, that of matter with $T = 0.9 T_c$ is reduced when further increasing ΔT from $0.01 T_c$ to $0.1 T_c$, cf. Figs. 8 (b) and (c). The lifetime of cooler matter with $T \leq 0.7 T_c$ is not appreciably influenced around $\epsilon_0 = \epsilon_Q$.

In order to understand this reduction of the lifetime for increasing ΔT , we show in Fig. 9 the time evolution of the temperature at $x = 0$ for various values of ΔT and an initial energy density $\epsilon = 50 T_c s_c / 2(r + 1) = 1.875 T_c s_c$. This value is close to the softest point of the equation of state, i.e., where the above mentioned effects on the lifetime are most drastic. In this representation, the rather long lifetime of matter with temperature $T = T_c$ ($t_{life} \simeq R/|v_{sh}| \simeq 43 R$) for a sharp first order phase transition can be seen in a particularly clear way. This *temporal* temperature profile changes *smoothly* with increasing ΔT . The *drastic* effect on the lifetime of matter with $T = T_c$ and $T = 0.9 T_c$ observed in Fig. 8 is readily explained via Fig. 9 as follows. For $\Delta T = 0$ the temperature stays constant (and equal to T_c) over a rather long period of time $\sim 43 R$, due to the small velocity of the rarefaction shock which consumes mixed phase matter and consequently takes a long time

to reach the center $x = 0$, cf. Fig. 5 (a). After that, the temperature drops sharply, cf. also Fig. 5 (g).

For small finite $\Delta T = 0.01 T_c$, however, the temperature is *already slowly decreasing with time*, cf. also Figs. 5 (b,e). This leads to a much shorter lifetime of matter with the particular temperature $T = T_c$, although the system remains obviously rather hot, $T \simeq T_c$, for a time span $\sim 37 R$ that is only slightly smaller than in the previous case. This also accounts for the long lifetime of matter with $T = 0.9 T_c$ as observed in Fig. 8 (b). After that time, the cooling is again rather drastic due to the rarefaction shock which has then reached the center $x = 0$. For increasing ΔT , the cooling of hot matter becomes faster, which explains why the lifetime of matter with $T = 0.9 T_c$ is eventually also appreciably reduced, cf. Fig. 8 (c).

One also notes that the lifetime of matter with $T = 0.7 T_c$ is not much influenced when increasing ΔT , in accord with our above observation in Fig. 8. On the other hand, matter with even lower temperatures may survive longer. In general, the more rapid cooling of matter with higher temperatures as well as the delayed cooling of matter with smaller temperatures is well explained by the increasing “stiffness” of the equation of state at higher energy densities and its “softening” at smaller energy densities for increasing ΔT , cf. Fig. 2 (b).

An important conclusion to be drawn from Figs. 8 and 9 is that for increasing ΔT the maximum in the lifetime of matter with temperature around T_c vanishes and that, for $\Delta T = 0.1 T_c$, there is no longer any irregularity that can be traced to the rapid variation of thermodynamical quantities in the phase transition region. In fact, in that case the shapes of the lifetime curves resemble those for the expansion of an ideal gas, cf. Figs. 8 (c) and (d). However, the existence of a transition from hadronic to quark and gluon degrees of freedom, the softening of the equation of state induced by that transition, and the resulting delayed expansion causes the lifetimes to be larger by an overall factor ~ 10 , cf. also Fig. 9. We will discuss possible implications for proposed quark–gluon–plasma signatures in the next section.

The curves in Fig. 8 (d) could also be calculated analytically employing Landau’s solution [20] which gives

$$t|_{x=0} = \left. \frac{\partial \chi(T, \alpha)}{\partial T} \right|_{x=0}, \quad (12)$$

where

$$\chi(T, \alpha) = -\frac{TR}{c_s} \int_{c_s \alpha}^{\ln[T_0/T]} du e^{(1+\beta)u} I_0 \left(\beta \sqrt{u^2 - c_s^2 \alpha^2} \right). \quad (13)$$

Here $\beta \equiv (1 - c_s^2)/2c_s^2 = 1$ for $c_s^2 = 1/3$ and $\alpha \equiv \tanh v$ is the fluid rapidity. At $x = 0$ we also have $\alpha = 0$ by symmetry and we obtain

$$t|_{x=0} = \frac{R}{c_s} \left\{ \left(\frac{T_0}{T} \right)^2 I_0(\ln[T_0/T]) - \int_0^{\ln[T_0/T]} du e^{2u} I_0(u) \right\}. \quad (14)$$

To understand the qualitative behaviour of the curves in Fig. 8 (d), it is sufficient to note that the integral is always dominated by contributions from the upper boundary. For $T_0 \gg T$ one may thus use the asymptotic approximation $I_0(u) \sim e^u$ in the integrand and obtains

$$t|_{x=0} \equiv t_{life} \sim R T_0^3 \sim R \epsilon_0^{3/4} \quad (15)$$

for fixed T . Thus, t_{life}/R behaves (at least asymptotically) $\sim \epsilon_0^{3/4}$ independent of T/T_c . This behaviour is in accord with the one observed in Fig. 8 (d). Curves for different T/T_c are simply shifted due to different constants of proportionality. Note that an increase of the lifetime proportional to $\epsilon_0^{3/4}$ is also expected in scaling hydrodynamics [14].

4.2 Variable $R(\epsilon_0)$

In Fig. 8 R was assumed fixed for all initial energy densities. Now we allow it to vary with ϵ_0 to take into account the Lorentz contraction of the colliding nuclei. To specify this relationship quantitatively, we consider two models for the initial stage of central $A + A$ -collisions.

The first is the scenario employed in [15]. It is assumed that half of the available CM energy, $\sqrt{s} = 2AM_N\gamma_{CM}$, is deposited in a cylinder of height $2R_A/\gamma_{CM}$ and radius R_A . Thus, $\epsilon_0 = AM_N\gamma_{CM}^2/2\pi R_A^3$. The initial “radius” of the system is therefore

$$R = \frac{R_A}{\gamma_{CM}} = \frac{R_A}{(\epsilon_0/T_c s_c)^{1/2}} \left(\frac{AM_N}{4\pi(r+1)p_c R_A^3} \right)^{1/2}. \quad (16)$$

With $p_c = \pi^2 T_c^4/30$, $T_c = 170$ MeV⁵, and $R_A = 1.12 A^{1/3}$ fm, this leads to $R/R_A \simeq 0.334 (\epsilon_0/T_c s_c)^{-1/2}$. Fig. 10 shows the results of Fig. 8 with the t_{life}/R -scale converted according to this formula. One observes that the lifetime in units of the radius R_A of the nucleus does not grow as rapidly with the initial energy density as in Fig. 8, due to the fact that the system’s initial size is shrinking with the CM-frame Lorentz-gamma (leading to the factor $\epsilon_0^{-1/2}$ in (16)). This suppression of the lifetime at high ϵ_0 has the interesting effect that existing maxima in the lifetime of different temperatures as observed in Fig. 8 are *enhanced* in Fig. 10. In the case $\Delta T = 0.1 T_c$, even new maxima are *created* for $T = 0.7$ and $0.9 T_c$. The reduction of the lifetimes of matter with temperatures near T_c for increasing ΔT is, of course, not influenced by the rescaling of the t_{life}/R -axis.

On the other hand, in the ideal gas case, Fig. 10 (d), the rescaling of the t_{life}/R -axis creates a *minimum*. This can be understood as follows. For large ϵ_0 we may employ the asymptotic formula (15) and note that $R \sim \epsilon_0^{-1/2}$ according to (16), which results in $t_{life} \sim \epsilon_0^{1/4}$, i.e., a weak increase with ϵ_0 as observed in Fig. 10 (d). For small ϵ_0 , we employ (14) with $T \simeq T_0$, which results in $t_{life} \sim R \sim \epsilon_0^{-1/2}$, i.e., a decrease with ϵ_0 . The two different forms give rise to the observed minimum at a certain value of ϵ_0 which increases for increasing T/T_c , since the asymptotic behaviour $T_0 \gg T$ is then realized only for correspondingly larger values of $\epsilon_0 \sim T_0^4$. The qualitative difference in the behaviour seen in Fig. 10 (c) as compared to Fig. 10 (d) contrasts sharply the similarity of Figs. 8 (c) and (d). The maxima in Fig. 10 (c) and the minima in Fig. 10 (d) are, however, not prominent enough to be of relevance for quark-gluon-plasma signatures. On the other hand, the huge quantitative difference in the lifetimes (a factor of ~ 10), which is, of course, still present, could have consequences for observables (see next section).

⁵This value is slightly larger than the one cited in the Introduction, but still consistent with lattice QCD calculations, cf. the discussion in [7]. We choose this value mainly to maintain consistency with [16, 24].

For the second scenario, we employ the one-dimensional shock model [22, 24]. Since we presently consider baryon-free matter only, we model the “ground state” of the colliding nuclei as a (massless) pion gas at $T \simeq 143$ MeV, i.e., with pressure $p_i = p_c/2$. The energy density ϵ_0 of the hot, compressed state is determined by solving the integral conservation laws for energy and momentum across the shock [4]. This gives also values for the shock velocity v'_{sh} in the rest frame of incoming matter

$$v'_{sh} = \left(\frac{p_0 - p_i}{\epsilon_0 - \epsilon_i} \frac{\epsilon_0 + p_i}{\epsilon_i + p_0} \right)^{1/2}, \quad (17)$$

and the CM velocity v_{CM} of matter required to reach that particular energy density,

$$v_{CM} = \left(\frac{p_0 - p_i}{\epsilon_0 + p_i} \frac{\epsilon_0 - \epsilon_i}{\epsilon_i + p_0} \right)^{1/2}. \quad (18)$$

The CM time when the complete “nucleus” is compressed (or the shock front has traversed the incoming nucleus, respectively) is calculated as [13, 24]

$$\frac{t_F}{R_A} = \frac{(1 - v'_{sh}v_{CM})\gamma_{CM}}{v'_{sh}}. \quad (19)$$

This time is (up to a factor $c = 1$) identical to the initial “radius” R of the system. With equations (17) and (18) one can thus relate R to ϵ_0 , similar as in (16). One has, however, to consider that a single shock is not the hydrodynamically stable solution in thermodynamically anomalous matter [24]. The correct solution is a sequence of single shocks and simple compression waves and, as a consequence, the initial energy density of the system is no longer constant over its extension $2R$. For our purpose of obtaining a simple estimate of R as a function of ϵ_0 we will neglect these details and use a linear interpolation in the respective region of ϵ_0 -values. The resulting initial size R of the system as a function of ϵ_0 is shown in Fig. 11. With this $R(\epsilon_0)$ we then convert the t_{life}/R -scale in Fig. 8. The results are depicted in Fig. 12 and are qualitatively similar to Fig. 10. The rapid decrease of R above $\epsilon_0 \simeq \epsilon_Q$ for $\Delta T = 0$ and $0.01 T_c$ strongly enhances the maximum in the lifetime of matter with temperatures near T_c and even creates a maximum in the lifetime of matter with cooler temperature, cf. Figs. 12 (a,b). The maxima observed in Fig. 10 (c) are now also more pronounced, cf. Fig. 12 (c), while Fig. 12 (d) still exhibits minima as in the corresponding Fig. 10 (d). The one-dimensional shock model thus proves to be the most optimistic scenario for quark-gluon-plasma signatures that require the existence of a distinguished maximum in the lifetime of hot matter at the softest point of the equation of state, like the proposed enhanced emission of electromagnetic probes [15].

We conclude that the lifetime of matter with temperatures near T_c is rather sensitive to the choice of ΔT and decreases rapidly for increasing ΔT for initial energy densities around the softest point of the equation of state. On the other hand, regions of lower temperature ($T \leq 0.7 T_c$, cf. Fig. 9) are less sensitive to variations in ΔT and even survive longer with increasing ΔT . Both phenomena have been explained in terms of the change in the “stiffness” of the equation of state when varying ΔT . For a fixed initial system size (independent of ϵ_0),

increasing ΔT eliminates the maxima in the lifetime near the softest point of the equation of state (see Fig. 8 (c)). On the other hand, if one accounts for the Lorentz contraction of the initial size of the system, then such maxima in the lifetime persist even for finite ΔT . This is in contrast to the case without a phase transition, where the lifetimes rather exhibit minima for the corresponding values of ϵ_0 (Figs. 10, 12 (d)). The lifetimes are also much longer (a factor of ~ 10) in case a rapid change in the degrees of freedom occurs. Experimental implications will be discussed in the next section.

5 Summary and Conclusions

In this work we have studied the one-dimensional hydrodynamic expansion of a finite system with an equation of state featuring a transition between (baryon-free) hadronic matter (with 3 massless degrees of freedom) and a quark-gluon plasma (with 37 massless degrees of freedom). The system's evolution was studied as a function of its initial energy density ϵ_0 (which was assumed to be homogeneous) and the width ΔT of the phase transition region in the equation of state. For $\Delta T < \Delta T^*$, where $\Delta T^* \simeq 0.07676 T_c$, the equation of state has regions where matter becomes thermodynamically anomalous. Thus, rarefaction shock waves appear in the one-dimensional expansion, in contrast to the case $\Delta T \geq \Delta T^*$, where matter is thermodynamically normal for all energy densities and (overlapping) simple waves form the hydrodynamically stable expansion solution.

Temperature profiles are not very sensitive to ΔT for initial energy densities well above and below the softest point of the equation of state, in agreement with the results of [11]. Variations of ΔT have, however, an appreciable influence on the temperature profiles for ϵ_0 near the softest point. In particular, rarefaction shocks are much weaker for finite ΔT than in the case $\Delta T = 0$ and transform into “bumps” resembling smeared shocks in the thermodynamically normal case $\Delta T \geq \Delta T^*$. The shock strength is much smaller because, as shown via eq. (10), the region where matter is thermodynamically anomalous shrinks abruptly when ΔT becomes finite. The “bump” structures in the thermodynamically normal case appear due to the variation of the velocity of sound in the transition region. In general, the equation of state at high energy densities becomes increasingly stiffer for increasing ΔT , which leads to more rapid expansion and cooling of the hot parts of the system. On the other hand, it becomes softer at smaller energy densities and thus the cooler parts of the system expand less rapidly and keep their temperature longer.

The above results were obtained assuming one-dimensional geometry and neglecting the finite (net) baryon density in the stopping regime. Nevertheless, we consider possible experimental consequences that may apply also in more realistic situations. The most important consequence from the experimental point of view is that the lifetimes of matter with temperatures near T_c decrease rapidly with increasing ΔT , if ϵ_0 is in the vicinity of the softest point of the equation of state. This will have an effect on the electromagnetic signature proposed in [15]. For instance, the rate (per unit volume) of direct thermal photons with energy E emitted from quark-gluon matter (at rest) is given by [25]

$$E \frac{dR^\gamma}{d^3k} = \frac{5\alpha\alpha_S}{18\pi^2} T^2 e^{-E/T} \ln \left(\frac{2.912E}{g^2T} + 1 \right). \quad (20)$$

For a fixed photon energy of $E = 1$ GeV, a reduction of the temperature by $\sim 10 - 20\%$, as seen in Fig. 9 when ΔT increases from 0 to $0.1 T_c$, would reduce the number of photons by a factor of $\sim 2 - 4$ (for $T_c = 170$ MeV, $\alpha_S = 0.4$). In addition, the rate integrated over space-time will be smaller by an even larger factor, because the space-time volume of hot matter also shrinks for increasing ΔT , cf. Figs. 3 – 7 (g,h,i). This makes a direct thermal electromagnetic signal of the quark–gluon plasma much more difficult to disentangle from background sources. On the other hand, after taking into account the expected Lorentz contraction of the initial size of the system, *all* lifetimes assume a maximum as a function of ϵ_0 at the softest point of the equation of state, cf. Figs. 11, 12, independent of ΔT . The detection of this feature is, however, complicated by the broadening of this maximum with increasing ΔT .

The generic feature that remains *independent* of ΔT is that the lifetimes of matter of any temperature are larger by a factor of ~ 10 as compared to the ideal gas case. In this respect, the interferometric signal of such long lifetimes associated with a phase transition to the quark–gluon plasma [17] appears to be less sensitive to ΔT than hard electromagnetic probes.

Finally we comment on the signature proposed in Ref. [16], where it was shown that the excitation function of the directed transverse flow has a minimum generated by the softest point of the equation of state, or in other words, the minimum in the function p/ϵ . Such a minimum still exists even for finite ΔT , cf. Fig. 2 (b). However, the intrinsic dynamical mechanism for the decrease of the transverse directed flow was the inertness of the mixed phase that prevented it to expand and deflect spectator matter. This inertness is weakened at finite ΔT and hot matter in the phase transition region expands and cools much more rapidly than in the case of a strong first order phase transition, although still much slower than if there were no transition at all, cf. Figs. 8 (c) and (d). Further and more detailed, three-dimensional studies [26] are required before a definite conclusion of the effect on the transverse directed flow can be drawn.

Acknowledgments

We thank A. Dumitru for discussions and the Nuclear Theory Group at Brookhaven National Laboratory for hosting a summer workshop, where part of this work was done.

References

- [1] For a review see, for instance:
H. Stöcker and W. Greiner, Phys. Rep. 137 (1986) 277, and refs. therein,
R.B. Clare, D.D. Strottman, Phys. Rep. 141 (1986) 177, and refs. therein.
- [2] (3+1)-dimensional relativistic one-fluid-dynamics is applied, for instance, in:
U. Ornik, F.W. Pottag, R.M. Weiner, Phys. Rev. Lett. 63 (1989) 2641,
T.L. McAbee, J.R. Wilson, J.A. Zingman, C.T. Alonso, Mod. Phys. Lett. A 4 (1989) 983,
N.S. Amelin et al., Phys. Rev. Lett. 67 (1991) 1523,
B. Waldhauser et al., Z. Phys. C 54 (1992) 459,
D. Strottman, Nucl. Phys. A 566 (1994) 245c,
L.V. Bravina, N.S. Amelin, L.P. Csernai, P. Levai, D. Strottman, Nucl. Phys. A 566 (1994) 461c,
R. Venugopalan, M. Prakash, M. Kataja, P.V. Ruuskanen, Nucl. Phys. A 566 (1994) 473c.
- [3] Multi-fluid-dynamical models are discussed in:
A.A. Amsden, A.S. Goldhaber, F.H. Harlow, J.R. Nix, Phys. Rev. C 17 (1978) 2080,
L.P. Csernai et al., Phys. Rev. C 26 (1982) 149,
I.N. Mishustin, V.N. Russkikh, L.M. Satarov, Int. Rev. Mod. Phys. 5 (eds. L.P. Csernai, D.D. Strottman, World Scientific, Singapore, 1991), p. 180ff,
U. Katscher et al., Z. Phys. A 346 (1993) 209.
- [4] L.D. Landau, E.M. Lifshitz, “Fluid mechanics” (Pergamon, New York, 1959).
- [5] J.D. Bjorken, Phys. Rev. D 27 (1983) 140.
- [6] See, for instance:
M. Creutz: “Quarks, gluons and lattices” (Cambridge University Press, Cambridge, 1983).
- [7] See, for instance:
B. Petersson, Nucl. Phys. B (Proc. Suppl.) 30 (1993) 66, and refs. therein.
- [8] F.R. Brown et al., Phys. Rev. Lett. 65 (1990) 2491.
- [9] F. Karsch, Nucl. Phys. B (Proc. Suppl.) 34 (1994) 63, Phys. Rev. D 49 (1994) 3791.
- [10] Y. Iwasaki, K. Kanaya, S. Kaya, S. Sakai, T. Yoshie, preprint UTHEP-304, UTCCP-P-1, May 1995.
- [11] J.P. Blaizot, J.Y. Ollitrault, Phys. Rev. D 36 (1987) 916.
- [12] A. Chodos, R.L. Jaffe, K. Johnson, C.B. Thorn, V.F. Weisskopf, Phys. Rev. D 9 (1974) 3471.

- [13] K.A. Bugaev, M.I. Gorenstein, B. Kämpfer, V.I. Zhdanov, *Phys. Rev. D* 40 (1989) 2903.
- [14] D.H. Rischke, S. Bernard, J.A. Maruhn, preprint CU-TP-692, nucl-th/9404018, to be published in *Nucl. Phys. A*.
- [15] C.M. Hung, E.V. Shuryak, preprint SUNY-NTG-94-59, hep-ph/9412360.
- [16] D.H. Rischke, Y. Pürsün, J.A. Maruhn, H. Stöcker, W. Greiner, preprint CU-TP-695, nucl-th/9505014, submitted to *Heavy Ion Phys.*
- [17] S. Pratt, *Phys. Rev. C* 49 (1994) 2722, *Phys. Rev. D* 33 (1986) 1314, G. Bertsch, M. Gong, M. Tohyama, *Phys. Rev. C* 37 (1988) 1896.
- [18] L. Van Hove, *Z. Phys. C* 21 (1983) 93, M. Gyulassy, K. Kajantie, H. Kurki-Suonio, L. McLerran, *Nucl. Phys. B* 237 (1984) 477.
- [19] M. Asakawa, T. Hatsuda, preprint CU-TP-705, UTHEP-316, hep-ph/9508360.
- [20] L.D. Landau, *Izv. Akd. Nauk SSSR* 17 (1953) 51, in: “Collected papers of L.D. Landau” (ed. D. Ter-Haar, Pergamon, Oxford, 1965), p. 569–585, L.D. Landau, S.Z. Belenkii, *Uspekhi Fiz. Nauk* 56 (1955) 309, *ibid.*, p. 665–700.
- [21] B.L. Friman, G. Baym, J.P. Blaizot, *Phys. Lett. B* 132 (1983) 291.
- [22] V. Schneider et al., *J. Comput. Phys.* 105 (1993) 92.
- [23] G. Baym, B.L. Friman, J.P. Blaizot, M. Soyeur, W. Czyż, *Nucl. Phys. A* 407 (1983) 541.
- [24] D.H. Rischke, Y. Pürsün, J.A. Maruhn, preprint CU-TP-693, nucl-th/9404021, to be published in *Nucl. Phys. A*.
- [25] J. Kapusta, P. Lichard, D. Seibert, *Phys. Rev. D* 44 (1991) 2774, D.K. Srivastava, B. Sinha, *Phys. Rev. Lett.* 73 (1994) 2421, A. Dumitru et al., *Phys. Rev. C* 51 (1995) 2166.
- [26] D.H. Rischke, M. Gyulassy (in preparation).

Figure Captions:

Fig. 1: (a) the energy density (in units of $T_c s_c$) divided by $(T/T_c)^4$, (b) three times the pressure (in units of $T_c s_c$) divided by $(T/T_c)^4$, (c) the entropy density (in units of s_c) divided by $(T/T_c)^3$, and (d) the square of the velocity of sound as functions of T/T_c . The solid line with the discontinuity at $T = T_c$ in (a,c) corresponds to $\Delta T = 0$. In (b), this curve has a kink at $T = T_c$, and in (d) it is the flat line at $c_s^2 = 1/3$ (the point $T = T_c$ is an exception, there $c_s^2 = 0$). The other curves correspond to $\Delta T = 0.01 T_c$ (dotted), $\Delta T = 0.05 T_c$ (dashed), $\Delta T = 0.075 T_c$ (dash-dotted), and $\Delta T = 0.1 T_c$ (solid).

Fig. 2: (a) entropy density (in units of s_c), divided by $(T/T_c)^3$, (b) p/ϵ , (c) the velocity of sound squared, and (d) $\Sigma T s$ as functions of energy density (in units of $T_c s_c$). The different curves correspond to those in Fig. 1.

Fig. 3: (a,b,c) temperature profiles and (d,e,f) center-of-momentum frame energy density profiles for times $t = 0.75 n \lambda R$, $n = 0, 1, \dots, 7$ and an initial energy density of $\epsilon_0 = 3 T_c s_c / 2(r + 1) = 0.1125 T_c s_c \equiv \epsilon_H$. The profiles are alternately shown as full and dotted lines in order to better distinguish them. (g,h,i) show isotherms in the space–time diagram. The isotherms are labelled with the corresponding temperatures in units of T_c . Figs. (a,d,g) are for $\Delta T = 0$, (b,e,h) for $\Delta T = 0.01 T_c$, and (c,f,i) for $\Delta T = 0.1 T_c$.

Fig. 4: Same as in Fig. 3, for $\epsilon_0 = 1.125 T_c s_c$, i.e., $\epsilon_H < \epsilon_0 < \epsilon_Q = (4r - 1) T_c s_c / 2(r + 1)$. Profiles in (a–f) are for times $t = 4 n \lambda R$, $n = 0, 1, \dots, 7$.

Fig. 5: Same as in Fig. 3, for $\epsilon_0 = 1.875 T_c s_c \sim \epsilon_Q$. Profiles in (a–f) are for times $t = 6 n \lambda R$, $n = 0, 1, \dots, 8$.

Fig. 6: Same as in Fig. 3, for $\epsilon_0 = 3.75 T_c s_c \sim 2 \epsilon_Q$. Profiles in (a–f) are for times $t = 10 n \lambda R$, $n = 0, 1, \dots, 7$.

Fig. 7: Same as in Fig. 3, for $\epsilon_0 = 18.75 T_c s_c \gg \epsilon_Q$. Profiles in (a–f) are for times $t = 12.5 n \lambda R$, $n = 0, 1, \dots, 8$.

Fig. 8: The lifetime of differently hot parts of the system as a function of the initial energy density for (a) $\Delta T = 0$, (b) $\Delta T = 0.01 T_c$, (c) $\Delta T = 0.1 T_c$, and (d) an ideal gas equation of state with $c_s^2 = 1/3$. Full line and circles: lifetime of matter having temperature $T = 0.5 T_c$, dotted line and squares: $T = 0.7 T_c$, dashed line and diamonds: $T = 0.9 T_c$, long dashed line and triangles pointing upwards: $T = T_c$, dash-dotted line and triangles pointing downwards: $T = 1.1 T_c$, full line and stars: $T = 1.3 T_c$. Note the change in the scale of t_{life} in (d).

Fig. 9: Temperature (in units of T_c) at $x = 0$ as a function of time (in units of R) for $\epsilon_0 = 1.875 T_c s_c \sim \epsilon_Q$. Lines correspond to ΔT -values as in Figs. 1, 2. The dashed line corresponds to a calculation with an ideal gas equation of state, $c_s^2 = 1/3$.

Fig. 10: The same as in Fig. 8, except that t_{life}/R is converted to t_{life}/R_A according to eq. (16), where R_A is the radius of a nucleus at rest.

Fig. 11: The system’s longitudinal “radius” R in units of R_A as a function of the initial energy density in the one–dimensional shock model. Full line: $\Delta T = 0$, dotted line: $\Delta T = 0.01 T_c$, dashed line: $\Delta T = 0.1 T_c$, dash-dotted line: ideal gas equation of state. The straight parts of the full and dotted lines are a linear interpolation between the points where the hydrodynamically stable compression solution ceases to be a single shock due to the thermodynamically anomalous behaviour of the equation of state in the phase transition region.

Fig. 12: The same as in Fig. 8, except that t_{life}/R is converted into t_{life}/R_A according to Fig. 11.

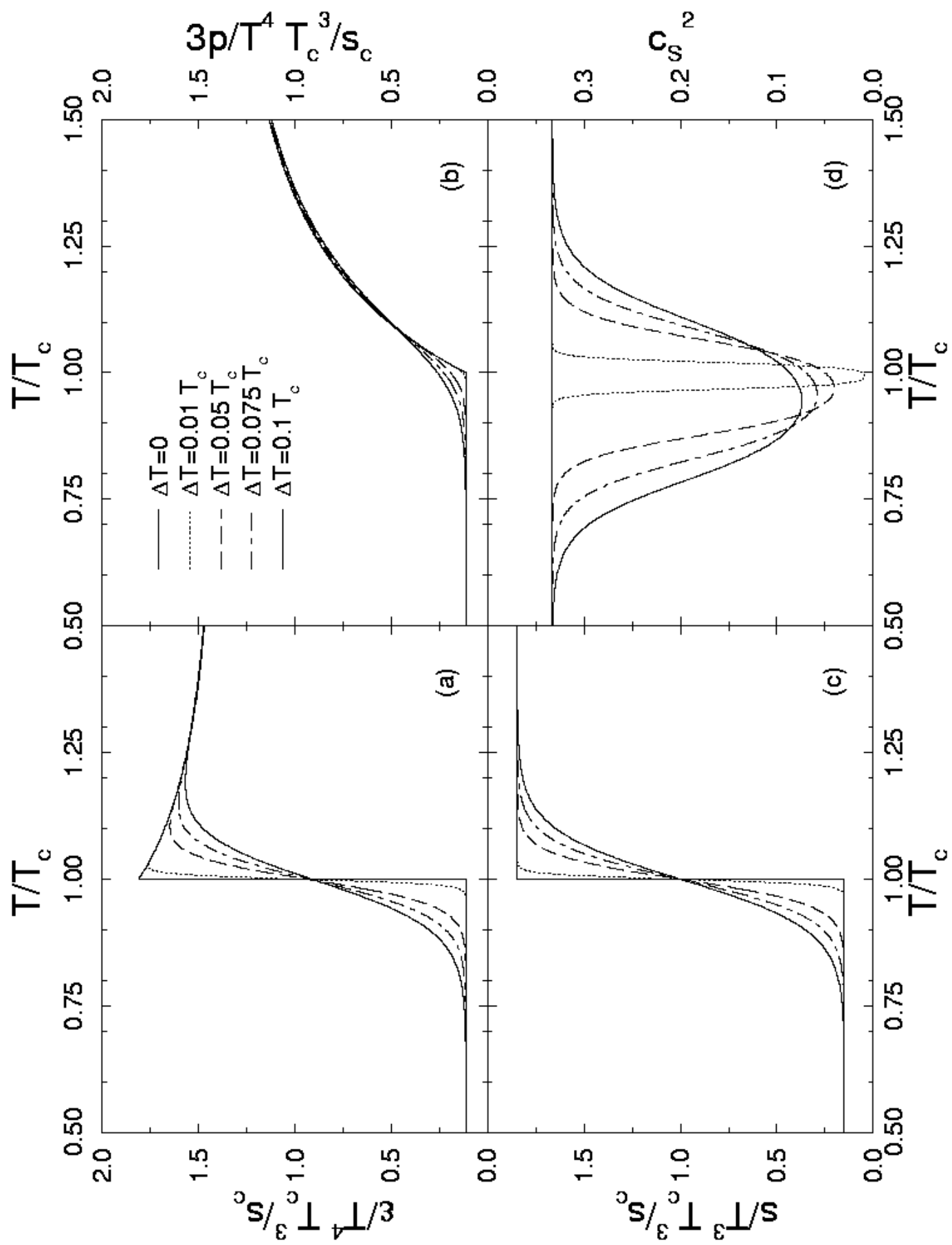


Fig.1

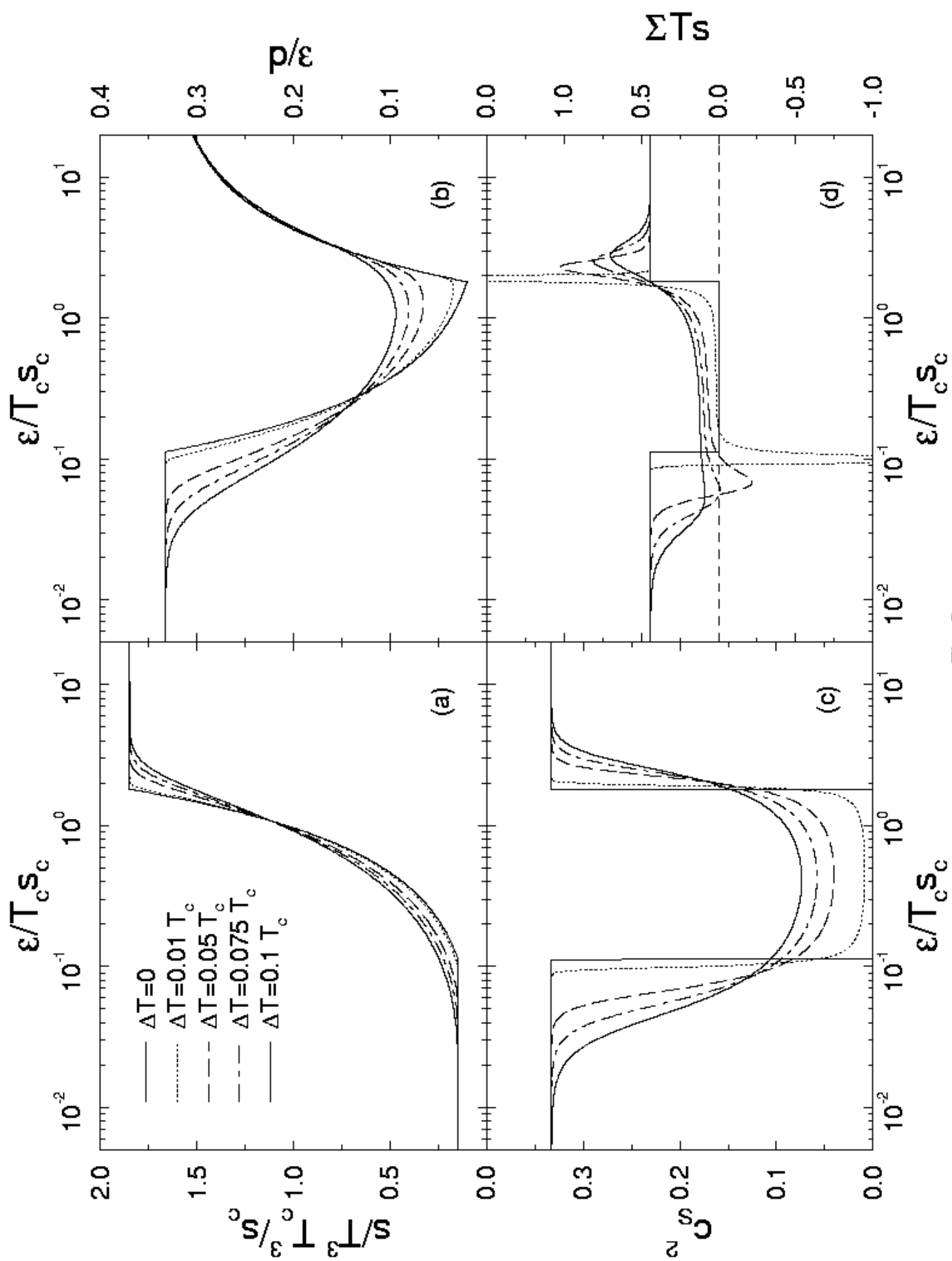


Fig.2

Fig.3

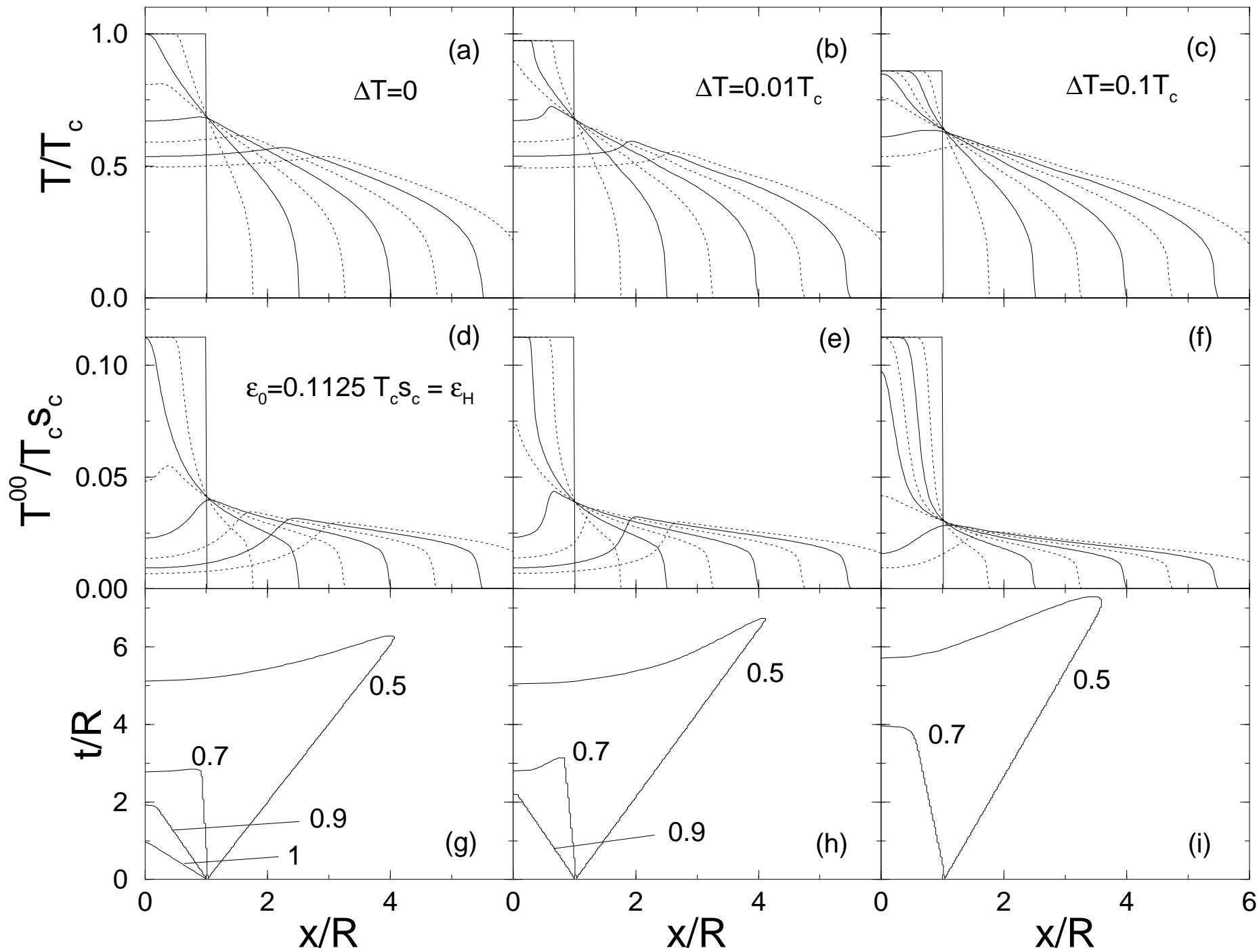


Fig.4

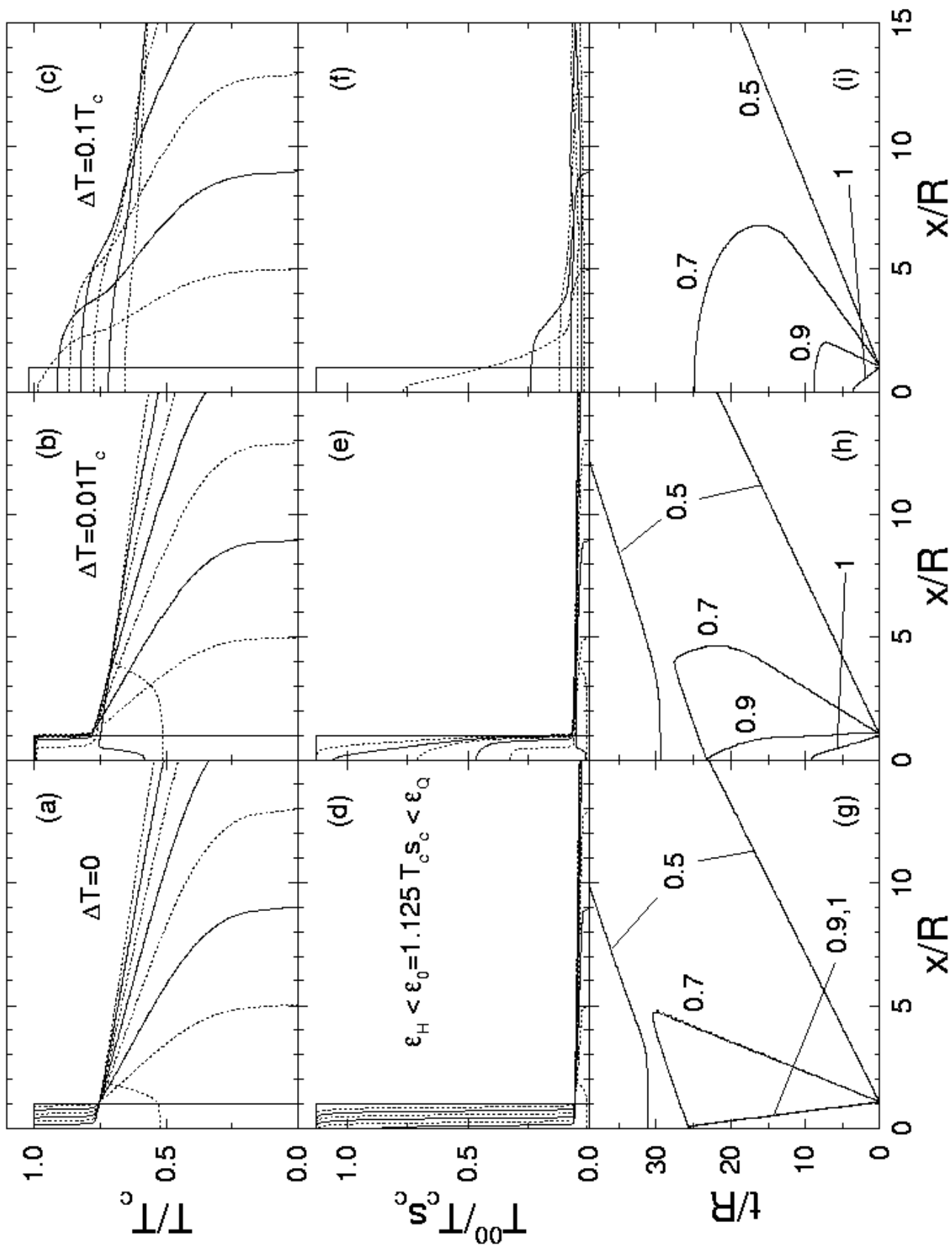


Fig.5

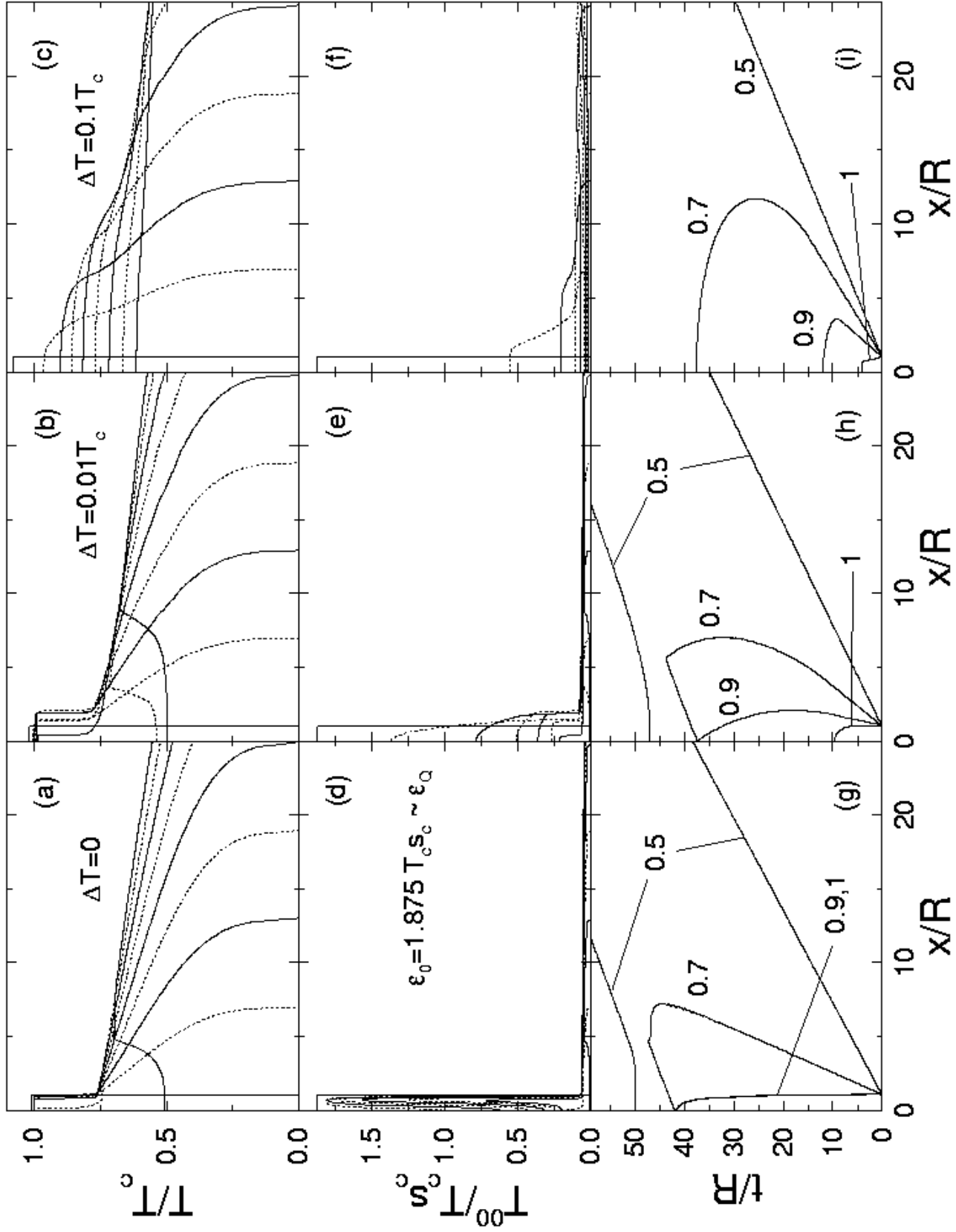


Fig.6

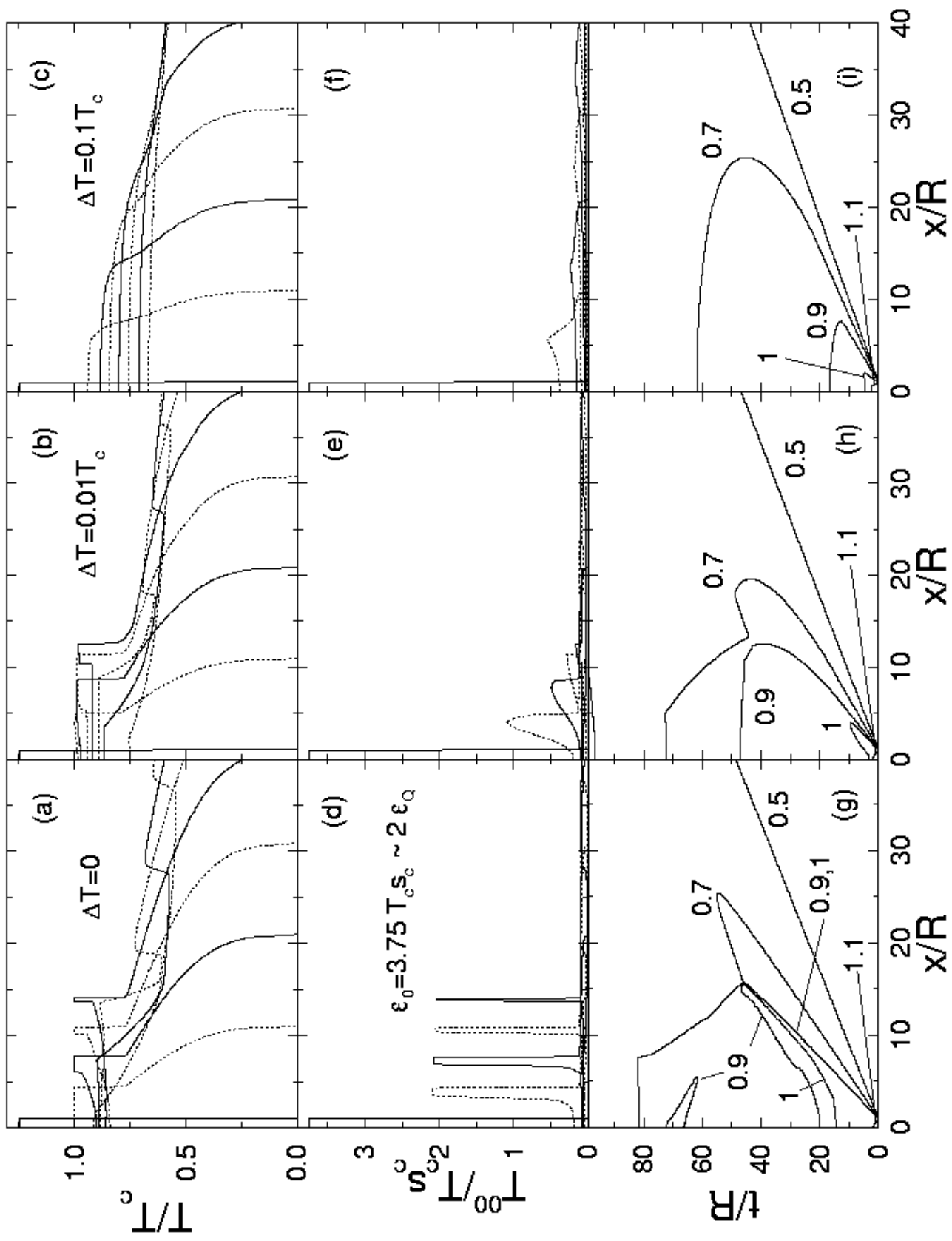


Fig.7

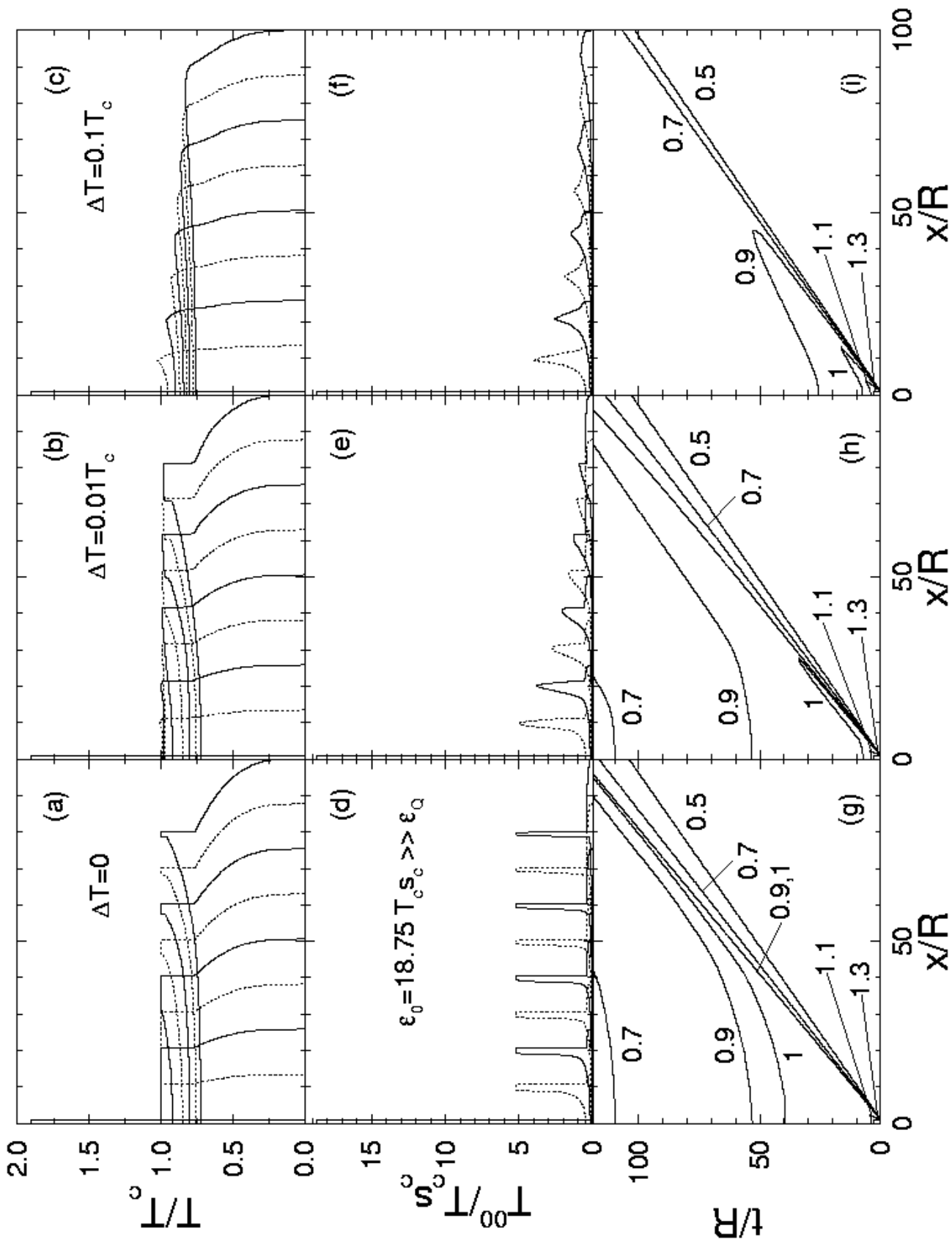


Fig.8

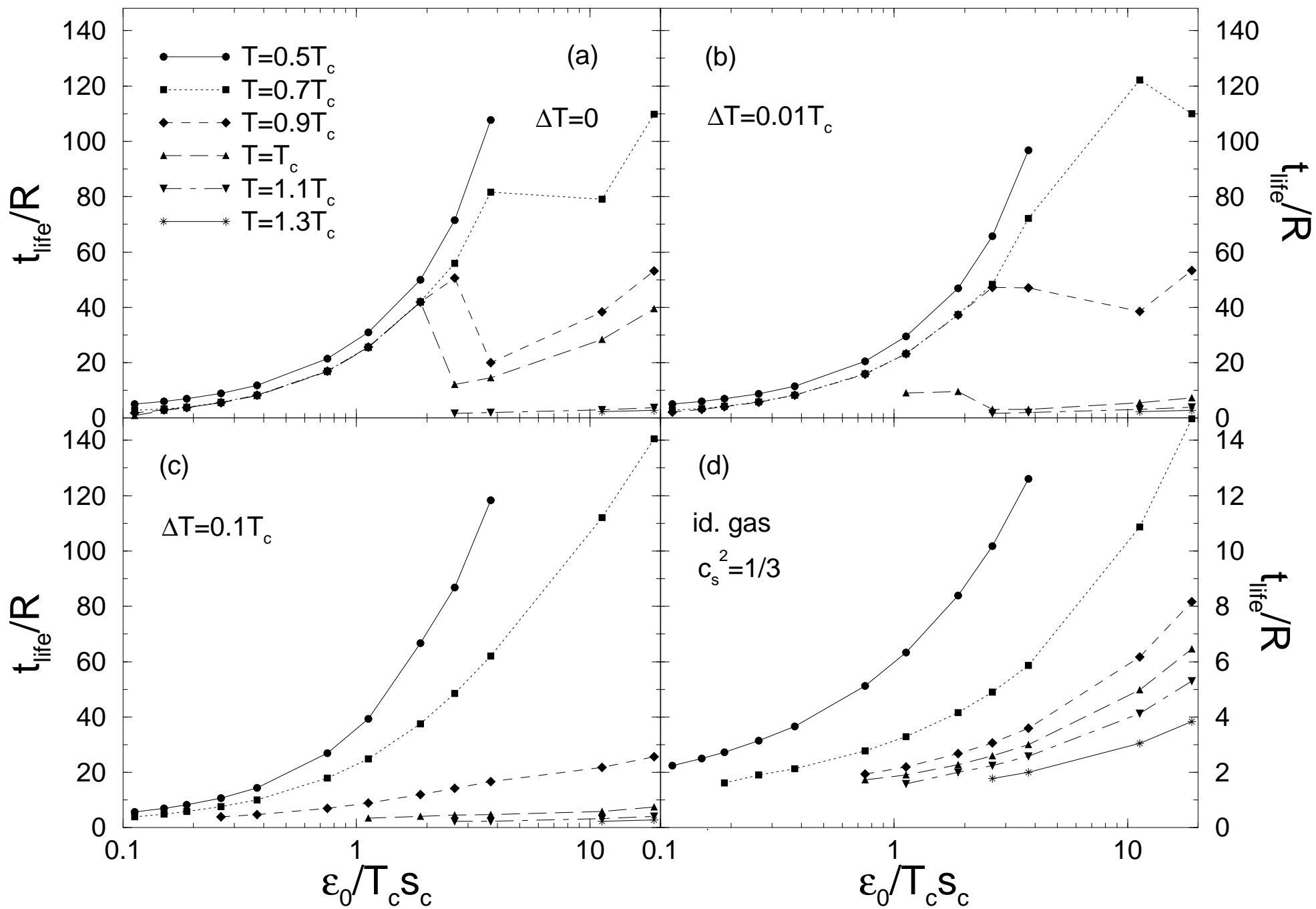


Fig.9

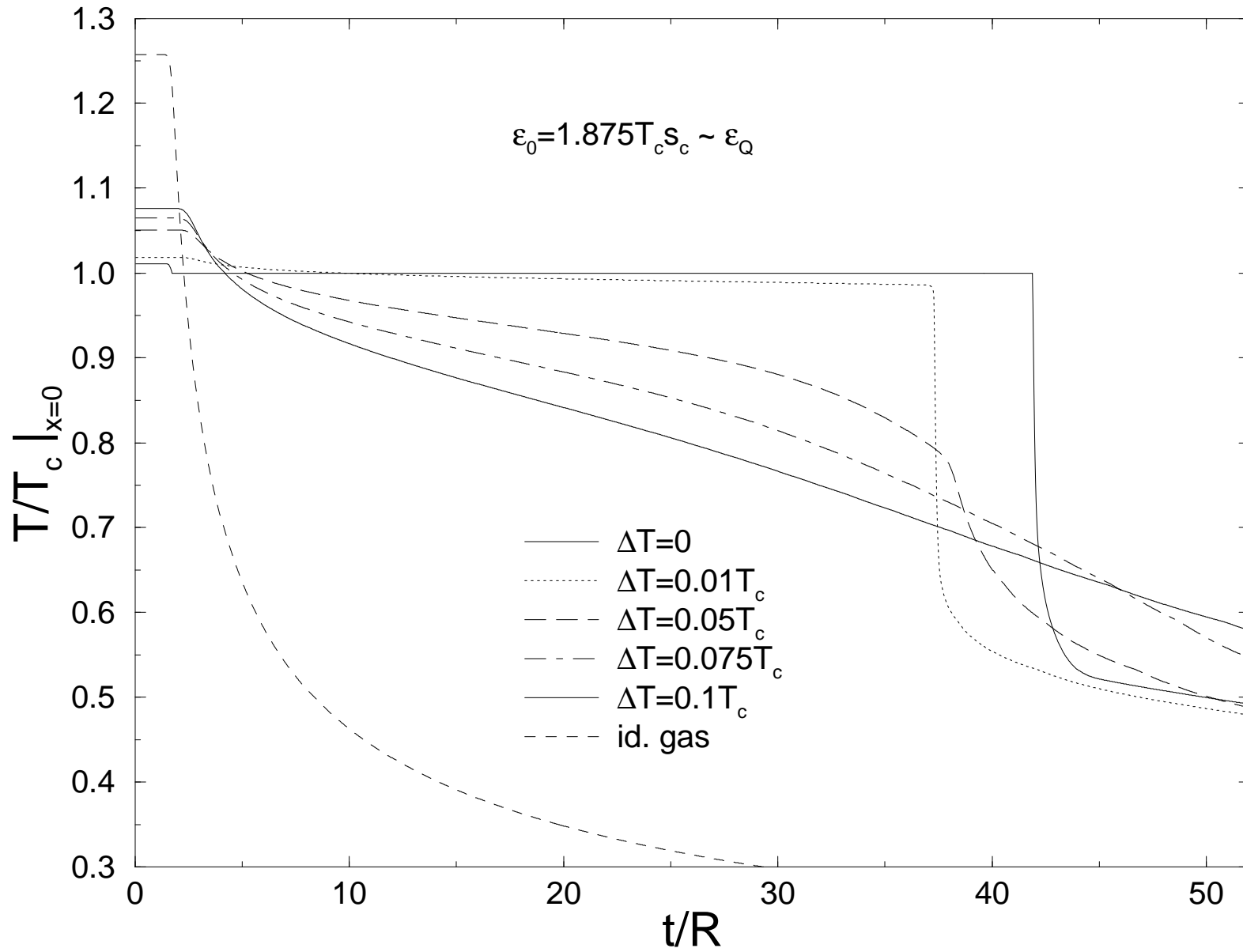


Fig.10

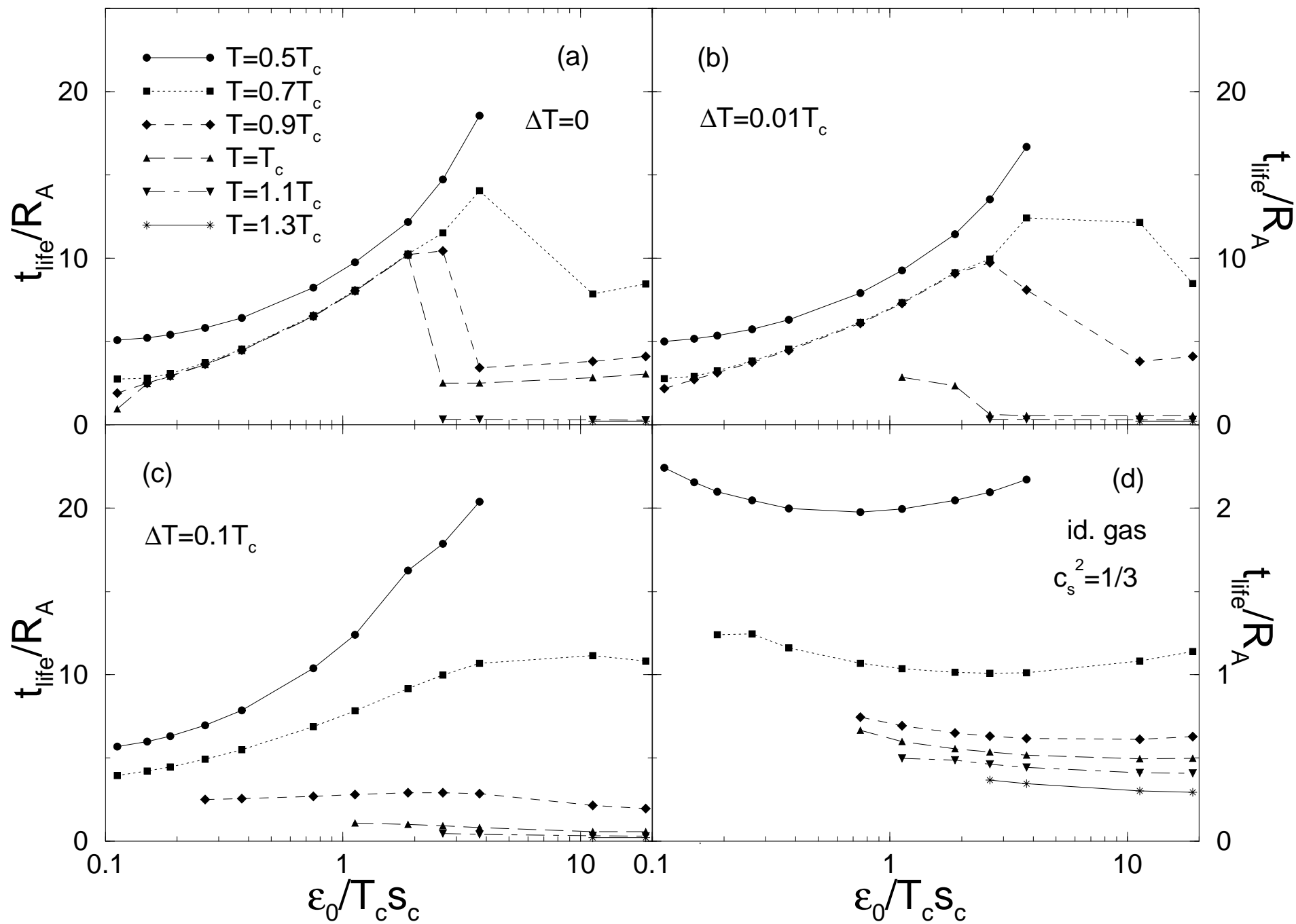


Fig.11

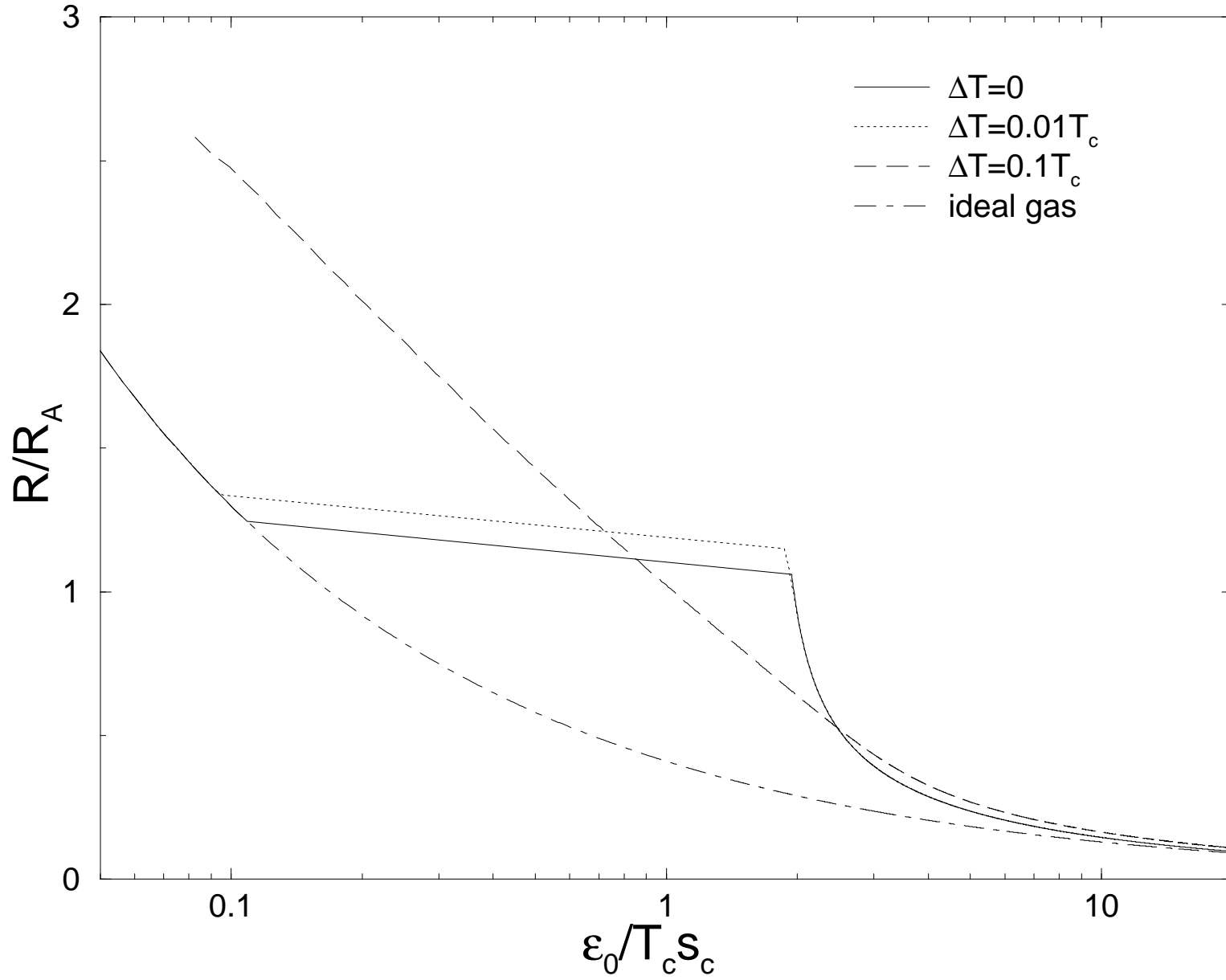


Fig.12

